symmetry

IMPACT FACTOR 2.2

CITESCORE 5.3

Article

Tachyonic AdS/QCD, Determining the Strong Running Coupling and β-Function in Both UV and IR Regions of AdS Space

Adamu Issifu, Elijah Anertey Abbey and Francisco A. Brito

Special Issue

Gravitational Physics and Symmetry

Edited by

Dr. Fabiano F. Santos and Dr. Moisés Felipe Bravo-Gaete

MDPI

https://doi.org/10.3390/sym18040682

symmetry

MDPI

Article

Tachyonic AdS/QCD, Determining the Strong Running Coupling and β-Function in Both UV and IR Regions of AdS Space

Adamu Issifu [1,2,3], Elijah Anertey Abbey [4] and Francisco A. Brito [5,6,*]

[1] Departamento de Física, Instituto Tecnológico de Aeronáutica, DCTA, São José dos Campos 12228-900, SP, Brazil; ai@academico.ufpb.br
[2] Laboratório de Computação Científica Avançada e Modelamento (Lab-CCAM), São José dos Campos 12228-900, SP, Brazil
[3] CFisUC, Department of Physics, University of Coimbra, 3004-516 Coimbra, Portugal
[4] Departamento de Física, Universidade Federal de São Carlos, Caixa Postal 676, São Carlos 13565-905, SP, Brazil; elijah@df.ufscar.br
[5] Departamento de Física, Universidade Federal de Campina Grande, Caixa Postal 10071, Campina Grande 58429-900, PB, Brazil
[6] Departamento de Física, Universidade Federal da Paraíba, Caixa Postal 5008, João Pessoa 58051-970, PB, Brazil
* Correspondence: fabrito@df.ufcg.edu.br

Abstract

In this paper, we investigate the Quantum Chromodynamics (QCD)-like running coupling, $\alpha_s^{AdS}(Q^2)$, and its associated β-function within a tachyonic Anti-de Sitter (AdS)/QCD framework. The AdS_5 bulk geometry is deformed through the introduction of a color dielectric function $G(\phi(z))$, associated with a tachyon field $\phi(z)$. This function governs the behavior of $\alpha_s^{AdS}(Q^2)$ across all momentum scales by modifying the AdS background at both small and large values of the holographic coordinate z. In the ultraviolet (UV) regime (small z), the deformation is driven by free tachyons and reproduces features consistent with perturbative QCD. In contrast, in the infrared (IR) regime (large z), tachyon condensation dominates, yielding behavior characteristic of nonperturbative QCD. This construction enables a unified description of the running coupling and its β-function over the full range of momentum transfer Q^2, where Q^2 denotes the space-like momentum scale.

Keywords: AdS/QCD; tachyon condensation; running coupling; β-function; nonperturbative QCD

1. Introduction

AdS/CFT correspondence [1,2] has attracted considerable attention in recent years. This duality scenario enables us to establish a relation between quantum gravity on $d+1$-dimensional Anti-de Sitter (AdS) space and d-dimensional conformal field theory (CFT). In principle, we can calculate physical observables in strongly coupled gauge theory in terms of weakly coupled classical gravity theory. One of the most intriguing examples [3] of the duality is the correspondence between SU(N) $\mathcal{N}=4$ supersymmetric Yang–Mills (SYM) theory and gravity. The correspondence is the basis for initiating holographic principles by 't Hooft [4]. The gravitational dual is type IIB supergravity or string theory [5]. This correspondence has proven to provide a supergravity explanation for field theories that display confinement and chiral symmetry-breaking characteristics [6,7]. The gauge theory dual to the AdS space has shown that the potential between two static color point particles has a Coulombic contribution to the net potential behavior [8,9], indicating a deconfinement phase transition. Furthermore, the investigation presented in [10] suggests that, when

Academic Editor: Jorge Segovia

Received: 12 February 2026
Revised: 11 April 2026
Accepted: 14 April 2026
Published: 20 April 2026

considering a compact boundary, AdS corresponds to the confinement phase while the black hole solution in AdS corresponds to the deconfinement phase. This interesting outcome is associated with the Hawking–Page transition [11], where two distinct solutions to the Einstein equations—AdS space and the AdS black hole—are considered.

Also, QCD phenomenology derived from holographic models has been applied successfully in studying several strong-interaction characteristics, such as light-flavor mesons [12] and glueball phenomenology [13] using a more robust approach referred to as configurational entropy [14–17].

In the AdS/CFT correspondence [1–3], the effective string tension T_{string} and the string coupling g_s are related through the 't Hooft coupling $\lambda := g^2N$ as $g_s = \lambda/(4\pi N)$ and $T_{\text{string}} = \sqrt{\lambda}/(2\pi)$ [18,19]. Thus, $g_s = g^2/4\pi$, where g is the gauge coupling of the SYM theory. In the limit $N \to \infty$, $g_s \to 0$, so perturbative string theory is applicable. On the other hand, in the limit $\lambda \to 0$ (weak gauge coupling), perturbation theory in terms of Feynman diagrams applies to the gauge theory [18,19]. In the 't Hooft limit $N \to \infty$, $\lambda =$ fixed, the spacetime curvature $\mathcal{R}$ is much smaller than the string scale $1/g_s$, so gravity provides a good approximation to the gauge theory. Otherwise, both theories are highly complex, making their equivalence nontrivial. Also, small curvature $\mathcal{R}$ means a large AdS radius R, since $\mathcal{R} \sim 1/R^2$, with $R = (4\pi g_s N)^{1/4} l_s$, where l_s is the string length [3]. The gauge and the string couplings are related by $g_s \sim g^2$, and in the 't Hooft limit, the string coupling becomes so small that stringy effects decouple. In this limit, non-planar interactions are removed, so we consider free strings on the $AdS_5 \times S^5$ background. Additionally, large N does not directly correspond to QCD; however, in many instances, results for large N are qualitatively similar to those for $N_c = 3$, where N_c is the number of colors in QCD. The 't Hooft parameter λ divides large-N QCD into two regions. In the limit $\lambda \ll 1$, we have a perturbative theory where Feynman diagrams are used to calculate amplitudes. In the limit $\lambda \gg 1$, we have strong coupling with non-planar diagrams [20]. Also, light-front holography establishes a relationship between the boost-invariant light-front wavefunctions and bound-state amplitudes in AdS space [21,22]. Holographic QCD provides a suitable description of hadrons with known spectroscopic dynamical characteristics [23,24].

In this work, we deform the AdS space [25–30] with a Higgs-like dimensionless *color dielectric function* $G(\phi)$ associated with a tachyonic potential [31–34]. The color dielectric function deforms the AdS space in the UV region in the presence of free tachyons (active tachyons), while the tachyon-condensed color dielectric function $G(\eta)$ (where η is the condensed tachyon field) also deforms the AdS space in the IR region, similar to the positive-sign dilaton profile used in determining strong couplings in AdS/QCD. The AdS action intended for this study is formulated from the Dirac–Born–Infeld (DBI) action modified at a tachyonic vacuum, similar to Sen's AdS_5 tachyonic action [35]. Firstly, we investigate the characteristics of both the strong running coupling $\alpha_s(Q^2)$ and the associated β-function $\beta(Q^2)$ by distorting the AdS space with the tachyonic $G(\phi)$. Secondly, we examine $\alpha_s(Q^2)$ and $\beta(Q^2)$ by distorting the AdS space with $G(\eta)$. We expect $\alpha_s(Q^2)$ and $\beta(Q^2)$ to behave similarly to perturbative QCD (pQCD) for the UV deformation of the AdS space. On the other hand, we expect AdS/QCD or nonperturbative QCD-like behavior for the IR deformation of the AdS space. The results obtained from these regions will be compared with effective couplings determined from different observables, such as lattice QCD results, QCD phenomenology, and the g_1 scheme, where $\alpha_{g1}(Q^2)$ is extracted from the well-measured Bjorken sum rule [36–49]. This approach provides a new perspective on AdS/QCD, in which pQCD coupling constants can be determined directly from a UV deformation of the AdS space rather than from extrapolation from an IR deformation. Also, we study the parameter that controls the transition from pQCD to nonperturbative QCD.

We present a unified holographic framework in which a Higgs-like tachyon potential deforms the AdS geometry through a single color dielectric function $G(\phi)$. In this approach, the deformation due to free tachyon modes governs the UV regime, yielding a decreasing coupling, $\alpha_s^{\text{AdS}}(Q^2)$, that connects the IR non-perturbative regime to the intermediate energy region where the gluon condensate changes sign, and the coupling approaches the perturbative domain. Unlike models that extrapolate from the IR to the UV (e.g., see a comprehensive review in [50]), this method derives both the perturbative and nonperturbative behaviors directly from the corresponding geometric deformations, establishing a continuous and unified description across all momentum scales without interpolation.

Additionally, we show that $\alpha_s(Q^2)$ and $\beta(Q^2)$ are related to scalar glueballs with mass m_ϕ in the IR regime or the tachyonic mass scale $\tilde{m}_\phi$ in the UV regime, and discuss their effect. We discuss any *Landau singularity* that may be observed in the UV region and propose how to deal with it in the model framework. The strong running coupling is a subject of active research due to its limited understanding in the low-momentum transfer region. Good knowledge of $\alpha_s(Q^2)$ at $Q \to \infty$ is necessary to match the growing precision of hadron scattering experiments and to enhance the understanding of high-energy unification of strongly interacting and electroweak theories. On the other hand, a precise understanding of $\alpha_s(Q^2)$ at $Q \to 0$ on the scale of the proton mass enables us to understand hadron structure, confinement, and hadronization [50–53] (and references therein).

This paper is organized as follows. In Section 2, we review well-known holographic QCD in two subsections: in Section 2.1, we review light-front holography, and in Section 2.2, we review AdS/CFT and holographic QCD. We set the basis for the study in Section 3; under this section, we discuss confinement at the tachyonic vacuum in Section 3.1, and the tachyonic AdS/QCD action in Section 3.2. We proceed to present the deformation of the AdS space in the UV region in Section 4, under which we discuss the strong running coupling in Section 4.1 and the β-function in Section 4.2. In Section 5, we study the deformation of the AdS space in the IR region, leading to the study of the associated strong running coupling in Section 5.1 and β-function in Section 5.2. We finalize by presenting our analysis and conclusion in Section 6, with the analysis in Section 6.1 and the conclusion in Section 6.2.

2. Review of Holographic QCD

2.1. Light-Front Holography

Light-front (LF) quantization [54,55] provides suitable grounds for investigating the structure of the hadrons concerning quark and gluon degrees of freedom. The LF wavefunctions (LFWFs) are the relativistic generalization of the Schrödinger wavefunctions. They are determined at fixed time $\tau = x^+ = x^0 + x^3$ referred to as the LF time [56] instead of the 'usual' fixed time t. LF holography [24,57–60] relates the equations of motion in AdS space to QCD Hamiltonian formalism in physical spacetime quantized on LF at τ. The correspondence allows for a direct relationship between the hadronic amplitude $\Phi(z)$ in AdS space and LFWF $\phi_L(\zeta)$ describing constituent quarks and gluons that form the hadron, with ζ the invariant impact LF variable. The connection is a consequence of AdS/CFT correspondence, a theory established to be scale-independent [3]. The term correspondence is applied because we can map a weakly interacting gravity-related theory in $d+1$-dimensional AdS space onto any strongly interacting CFT (such as SYM theory) in d-dimensions, giving rise to the name gauge/gravity duality. This mapping generates a relation between the 5th-dimension variable (z) of AdS space and ζ in physical spacetime.

The mapping between z and ζ was originally obtained by relating the electromagnetic current matrix element in AdS space [26] to the corresponding current matrix element in LF theory [24,61]. Also, we can establish a relationship between their energy-momentum

matrix elements [59]; this demonstrates the consistency of holographic mapping to physical observables in LF. The resulting equation for meson bound states $q\bar{q}$ at τ has the form of a single-variable relativistic Lorentz invariant Schrödinger equation

$$\left(-\frac{d^2}{d\zeta^2} - \frac{1-4L^2}{4\zeta^2} + U(\zeta)\right)\phi_L(\zeta) = \mathcal{M}^2\phi_L(\zeta), \tag{1}$$

where $\mathcal{M}$ is the mass, L is the relative orbital angular momentum of q (quark), and $\bar{q}$ (antiquark), $U(\zeta) = \kappa^4\zeta^2 + 2\kappa^2(L+S+1)$ is the confining potential in the soft-wall model with mass-scale κ and spin S. A full derivation of Equation (1) can be found in [60] and references therein. Therefore, when ζ is correctly defined, we can reduce the theory to a semi-classical approximation. In this case, the properties of the strong interacting dynamics are centered on an effective potential $U(\zeta)$ [50]. The advantage of LF holography is its direct geometric interpretation of confinement and the natural identification of the holographic coordinate ζ with the invariant impact variable of the LF wavefunctions, enabling a unified description of hadron spectra and the running coupling [24,60]. Compared to other holographic approaches, it provides a simpler and more transparent framework to describe the scale dependence of $\alpha_s(Q^2)$ across both UV and IR regimes [50,62].

The mapping between the AdS coordinate z and the physical light-front variable ζ is established by matching the AdS wave equation with Equation (1). For a two-particle bound state, the invariant impact variable $\zeta = \sqrt{x(1-x)}\,b_\perp$, where x is the longitudinal momentum fraction and $b_\perp$ the transverse separation, is identified with z up to a scale factor, i.e., $\zeta = z$. This relation is derived by comparing electromagnetic current matrix elements in AdS space with their light-front counterparts, yielding $z = \zeta$ in units where the AdS radius $R = 1$ [23,58,60].

2.2. AdS/CFT and Holographic QCD

QCD is neither conformal nor supersymmetric. However, it displays approximate conformal behavior in the far ultraviolet (UV) region, where quark–gluon degrees of freedom dominate, and in the deep infrared (IR) region, where the relevant degrees of freedom are hadronic. To capture color confinement, conformal symmetry in AdS_5 space must therefore be broken. The AdS/CFT framework relies on the isomorphism between the Poincaré group together with the conformal group SO(4,2) and the isometry group of AdS_5 space, with the AdS metric providing the geometric foundation for constructing QCD-like models.

$$ds^2 = \frac{R^2}{z^2}\left(\eta_{\mu\nu}dx^\mu dx^\nu - dz^2\right), \tag{2}$$

where R is the AdS radius. The metric is invariant under scale changes in the fifth-dimensional variable $z \to \tilde{\lambda}z$ and the spacetime variable $x^\mu \to \tilde{\lambda}x^\mu$. The z coordinate acts like a scaling variable in Minkowski space. Different values of z correspond to different measures of 4-momentum for which the hadron can be studied [62].

Some well-known functions that are introduced to break the AdS_5 space are dilaton profiles $e^{\pm\phi_d(z)}$, with $\phi_d(z)$ the dilaton field [23,63,64], or a warp factor $e^{A(z)}$, where $A(z)$ is any suitable function; commonly, logarithmic functions are used, i.e., $A(z) \sim \log(z)$. Whichever function is chosen to distort the AdS_5 space leads to *confinement* in uniquely different forms [65].

A particularly successful realization of this holographic approach is obtained by modifying the AdS_5 background with a positive-sign dilaton field, $\Phi(z) = +\kappa^2 z^2$. This profile leads to linear Regge trajectories, a confining potential, and a hadronic spectrum in excellent agreement with experimental data [23,30,62]. These changes induce an analytical

color confinement, leading to a nonperturbative AdS/QCD running coupling, $\alpha_s^{AdS}(Q^2)$. It is important to note that the understanding of the running coupling for pQCD is limited to short distances or high Q^2 regimes. In a similar sense, AdS/QCD with a positive dilaton background is based on long-distance interactions and the small Q^2 regime [62].

Analytically, the AdS_5 action bears resemblance to the general relativity action $S_{GR} \propto \int d^4x\sqrt{|\det g_{\mu\nu}|}\tilde{R}/G_N$, where $\tilde{R}$ is the Ricci scalar and G_N is Newton's constant. In AdS/QCD, we replace the Ricci scalar with the gauge field as $\sqrt{\tilde{R}} \to F^{\mu\nu}$, G_N is replaced by the gauge coupling $\sqrt{G_N} \to g_5$, and the modulus of the metric determinant $|\det g_{\mu\nu}|$ is replaced by the modulus of the AdS_5 metric determinant, $\sqrt{|\det g_{\mu\nu}|} \to \sqrt{|g_{AdS}|}e^{\kappa^2 z^2}$, which includes the dilaton profile $e^{\kappa^2 z^2}$ to distort the AdS_5 space; here, $\phi_d(z) = \kappa^2 z^2$ (see [50] for a more detailed analysis).

Therefore, the AdS_5 action takes the form

$$S_{AdS} = -\frac{1}{4}\int d^4x\, dz\, \sqrt{|g_{AdS}|}e^{\kappa^2 z^2}\frac{1}{g_5^2}F^{\mu\nu}F_{\mu\nu}. \tag{3}$$

From Equation (2), the determinant of the metric is $\sqrt{|g_{AdS}|} = (R/z)^5$ and from the above expression, after introducing the dilaton profile, it turns into $\sqrt{|g_{AdS}|}\cdot e^{\kappa^2 z^2} = (R/z)^5 e^{\kappa^2 z^2}$. The presence of the factor $e^{\kappa^2 z^2}$ breaks the conformal symmetry while the AdS_5 geometry remains unchanged. Therefore, the expression $(R/z)^5 e^{\kappa^2 z^2}$, makes the separation between $e^{\kappa^2 z^2}$ and the metric determinant, $(R/z)^5$, explicit. We emphasize that the dilaton field $\phi_d(z)$ enters the action as a multiplicative factor, $e^{\kappa^2 z^2}$, not as a modification of the metric determinant [23,62,63]. The prefactor

$$g_5^{-2}(z) = g_5^{-2}e^{\kappa^2 z^2} \tag{4}$$

restores the conformal symmetry in Equation (3) and leads to *color-confining* properties; in this case, g_5^2 has length dimension. Now, comparing g_5 to the coupling in the $\mathcal{N} = 4$ SYM theory g, and mapping $z \to \zeta$, we can calculate the AdS/QCD $\alpha_s^{AdS}(Q^2)$ and the associated $\beta(Q^2)$ [50].

The combination of these models discussed above follows a coherent logical progression: Light-front holography provides the fundamental identification between the AdS coordinate z and the physical impact variable ζ; the soft-wall model with a positive-sign dilaton minimally implements confinement and linear Regge trajectories; and the DBI action (discussed below) with a tachyonic potential offers a string-theoretic foundation that unifies the UV (free tachyon) and IR (condensed tachyon) deformations via a single color dielectric function. Each step builds on the previous one, resulting in a unified framework grounded in both phenomenology and string theory.

3. The Model

3.1. Confinement at Tachyonic Vacuum

We start from the Dirac–Born–Infeld (DBI) action [66–71] and extend it by including a tachyonic field near the tachyonic vacuum. In this regime, bosonic open strings effectively behave as closed strings without Dp-branes, as shown in string field theory: their endpoints are connected by flux lines on the Dp-brane worldvolume, forming closed strings [72–100].

From a quantum field theory viewpoint, Dp-branes do not vanish completely at the tachyonic vacuum but instead dissolve into lower-dimensional branes, which connect open-string endpoints and act as sources of color charge. In this limit, the negative tachyon potential $V(\phi)$ exactly cancels the Dp-brane tension ε_p, i.e.,

$$V(\phi) + \varepsilon_p = 0, \tag{5}$$

leaving no net energy cost for rearranging strings on the residual lower-dimensional branes and eliminating open string excitations [83–85,92,101–104].

In the present study, the relevant degrees of freedom are *valence gluons*. Consequently, the closed strings formed at the tachyonic vacuum are treated within the *color flux-tube picture* of QCD, consistent with *chromoelectric flux confinement* (see Ref. [105] and references therein).

The DBI action takes the form

$$S_{\rm DBI} = -T_p \int d^{p+1}\xi e^{-\phi_d} \sqrt{-\det(\eta_{\mu\nu} + (2\pi\alpha')F_{\mu\nu})}, \tag{6}$$

where $F_{\mu\nu} = \partial_\mu A_\nu - \partial_\nu A_\mu$ is the abelian gauge field strength living on the worldvolume of the Dp-brane, Dp-brane tension

$$\tau_p = \frac{T_p}{g_s} = \frac{1}{g_s\sqrt{\alpha'}(2\pi\sqrt{\alpha'})^p}, \tag{7}$$

string tension

$$T_{\rm string} = \frac{1}{2\pi\alpha'}, \tag{8}$$

and string coupling $g_s = e^{\langle\phi_d\rangle}$. To understand the strong interaction dynamics of the open strings on the Dp-brane worldvolume, we derive the dimensional reduced U(1) Yang–Mills theory [106,107] by small perturbation in Equation (6), which yields

$$S_{YM} = -\tau_p V_p - \frac{1}{4g_{YM}^2} \int d^{p+1}\xi F_{\mu\nu}F^{\mu\nu} + \mathcal{O}(F^4). \tag{9}$$

Here, V_p is the p-brane worldvolume, which can be ignored subsequently, and g_{YM} is the Yang–Mills coupling given by,

$$g_{YM}^2 = \frac{1}{(2\pi\alpha')^2\tau_p} = \frac{g_s}{\sqrt{\alpha'}}\left(2\pi\sqrt{\alpha'}\right)^{p-2}; \tag{10}$$

hence, the relation $g_{YM}^2 \sim g_s$, that forms the basis for the gauge/gravity duality is established. Since the mass of the string is proportional to its length, the closer the branes, the less massive the attached strings may be [71,108]. Therefore, for stacks of N Dp-branes, we have $\mathrm{U}(1)^N$ gauge groups on its worldvolume which can be decomposed as $\mathrm{U}(N) = \mathrm{SU}(N) \times \mathrm{U}(1)$. That can further be decomposed into standard model symmetry depending on the number of Dp-branes crossing each other [109–112]. Now, we modify Equation (6) with a tachyon potential $V(\phi)$ [113] to induce color confinement, with ϕ the tachyon field

$$\begin{aligned} S &= -T_p \int d^{p+1}\xi e^{-\phi_d} V(\phi) \sqrt{-\det(\eta_{\mu\nu} + (2\pi\alpha')F_{\mu\nu})} \\ &= -\tau_p \int d^{p+1}\xi V(\phi)\left[1 + \frac{1}{4}(2\pi\alpha')^2 F_{\mu\nu}F^{\mu\nu} + \mathcal{O}(F^4)\right]. \end{aligned} \tag{11}$$

In the last step, we considered slowly varying tachyons with a constant dilaton field $\langle\phi_d\rangle$. At the minimum of the potential $V(\phi_0)$, the action disappears [72,76,103]. Also, the potential is symmetric under $\phi_0 \to -\phi$, with maximum at $\phi = 0$ and minimum at $\phi_0 = \pm a$. We will disregard the first term and consider only the gauge fields propagating on the Dp worldvolume for the analysis, because the gauge field is enough for the current study.

The background dilaton field $\phi_d(z)$ is incorporated into the effective color dielectric function via $G(\phi, z) = e^{-\phi_d(z)}(2\pi\alpha')^2 V(\phi)$. Evaluated on-shell, this defines a scale-dependent coupling $G(\phi(z))$. Thus, the dilaton controls the z-dependence of the gauge coupling without modifying the AdS metric. This is consistent with standard soft-wall AdS/QCD treatments, where conformal symmetry breaking is encoded in background fields rather than in the geometry. Adopting the conventional normalization in string units, $(2\pi\alpha')^2 = 1$ and $\langle\phi_d\rangle$, the relation simplifies to $G(\phi) = V(\phi)$, rendering $G(\phi)$ dimensionless. Consequently, we have,

$$\mathcal{L} = -\frac{1}{4g_s} G(\phi) F_{\mu\nu} F^{\mu\nu}, \tag{12}$$

for $T_p = 1$. Introducing the kinetic energy component and the tachyon potential into the last step of Equation (11), we recover the Lagrangian density in references [31–34,114] used in studying color confinement.

Although the DBI gauge field is abelian, the non-abelian dynamics of QCD are captured by the holographic background [115,116]. In AdS/QCD, the running coupling is obtained from the two-point function of the gauge field strength, which reduces to a scalar problem in the isotropic background of the metric, dilaton, and tachyon [35]. The tachyon potential and color dielectric function encode the non-perturbative gluon dynamics, including confinement and the running of $\alpha_s(Q^2)$, in the same way as standard AdS/QCD models, where an abelian vector field [23,62] suffices to describe hadronic form factors and the QCD coupling. Thus, the abelian approximation [63,117] is fully adequate for computing $\alpha_s(Q^2)$, as the non-abelian structure is already incorporated through the background fields.

3.2. Tachyonic AdS/QCD Action

Considering 5D holographic QCD models, the background flavor branes are D4-$\bar{\text{D}}$4 systems [115,116,118,119]. In this study, we consider open strings with their endpoints on a Dp-brane worldvolume, so we consider a background D4-brane. Thus, we can express the AdS_5 action similar to the one proposed in [35] adopted in [120] for studying hadronic properties in the light of AdS/QCD, from Equation (11), as

$$S = -\frac{1}{4g_5^2} \int d^4x dz G(\phi(z)) F^{\mu\nu} F_{\mu\nu}, \tag{13}$$

where $G(\phi(z))$ is only a function of z and $g_s \to g_5^2$ has the dimension of length. Additionally, tachyonic corrections were introduced in Ref. [121] to show equivalence in AdS/QCD and tachyonic AdS/QCD [122] in 4D holographic dual to 5D weakly coupled gravity using a similar action. The $G(\phi)$ is carefully defined to induce confinement and asymptotic freedom in separate energy regimes. Again, we demonstrate that the *tachyonic color dielectric function*, $G(\phi)$, deforms the AdS_5 metric at the asymptotic AdS_5 bulk in the UV limit ($z \to 0$) corresponding to the deconfinement transition associated with AdS_5 black holes [11]. On the other hand, deforming the AdS_5 metric with *condensed tachyonic color dielectric function* $G(\eta)$ leads to IR deformation of the AdS_5 bulk, leading to the phenomenon of *color confinement* in the IR regime ($z \to \infty$), similar to deforming the 'usual' AdS_5 space with positive dilaton background [30]. Here, the confining transition corresponds to color singlet glueball states with N^0 degree of freedom, whilst the deconfinement transition corresponds to the state where the gluons are free with N^2 degrees of freedom [10,20].

Moreover, in the model framework, the tachyon field ϕ is dual to the scalar glueball operator $O = \text{Tr}\, G_{\mu\nu} G^{\mu\nu}$, as presented in Equations (18)–(20). At the false vacuum ($\phi = 0$), $\langle O\rangle \propto V(0) = \Lambda a^4/4$, while at the true vacuum ($\phi = \pm a$), the tachyon condenses, yielding $\langle O\rangle \propto a^4$, which encodes the gluon condensate in the confined phase. Fluctuations η around $\phi_0 = \pm a$ correspond to physical scalar glueball states with quantum numbers 0^{++}.

4. Deformation of the AdS Space in the UV Region

4.1. Strong Running Coupling

The strong running coupling $\alpha_s^{AdS}(Q^2)$ can be determined by defining a new coupling $g_5(z)$ with dependence on z, that restores the conformal symmetry in Equation (13) (this has been discussed extensively in Section 2.2),

$$g_5^{-2}(z) = g_5^{-2} G(\phi(z)). \tag{14}$$

This approach is similar to the one used in determining the QCD running coupling of AdS/QCD [50]. The deformation of the conformal symmetry in Equation (13) is relevant for obtaining running coupling and a nonzero β-function because conformal symmetry leads to constant coupling and zero β-function, similar to what is observed in classical QCD without quantum correction. The scale-dependent gauge field depicted by the expression above is equivalent to gauge field strength renormalization in the QCD theory. Here, the gauge field is scaled as $F^{\mu\nu} \rightarrow G^{1/2} F^{\mu\nu}$ to induce QCD-like properties.

In 'regular' QCD theory, we can rescale the gluon field as $A^\mu \rightarrow \tilde{\lambda} A^\mu$, which leads to $G^{\mu\nu} \rightarrow \tilde{\lambda} G^{\mu\nu}$, with $G^{\mu\nu}$ the non-abelian field strength, in the QCD Lagrangian density, $\mathcal{L}_{\rm QCD}$; this is accompanied by rescaling the coupling strength $g \rightarrow \tilde{\lambda}^{-1} g$. Thus, the renormalization of the physical QCD coupling $g_{phys} = Z_3^{1/2} g_0$ [123], with Z_3 the gluon propagator renomalization factor and g_0 the bare coupling in UV-regulated theory similar to renormalization of the gauge field and gauge field strength: $A^\mu_{ren} = Z_3^{-1/2} A^\mu_0$, $G^{\mu\nu}_{ren} = Z_3^{-1/2} G^{\mu\nu}_0$ resulting in a rescaled Lagrangian $\mathcal{L}^{ren}_{\rm QCD} = Z_3^{-1} \mathcal{L}^0_{\rm QCD} = (g_{phys}/g_0)^{-2} \mathcal{L}^0_{\rm QCD}$. All quantities with subscript or superscript '0' are bare and the ones with '*ren*' are their renormalized counterparts. A similar idea is applied in AdS/QCD calculations, where the regularized coupling is defined in terms of a suitable function that induces the QCD-like properties.

The nonconformal dynamics, confinement, and deconfinement transitions associated with QCD will now be investigated through $g_5(z)$, where $g_5(z) \rightarrow g_{YM}(\zeta)$—see Equation (9) for the comparison with YM theory. Therefore, we define the AdS_5 coupling constant, $\alpha_s^{AdS} \equiv g_5^2/4\pi$, which requires Q^2-dependence to fully describe the dynamics of the particles in both the UV and IR domains. What makes the $G(\phi)$ interesting is that it distorts the AdS_5 space curvature in two different forms, one in the UV regime and the other in the IR regime, so the perturbation and nonperturbative characteristics of the QCD-like coupling can be investigated in a single framework [62]. The α_s^{AdS} can be written in terms of the $G(\phi)$ as

$$\alpha_s^{AdS}(\zeta) = \frac{g_{YM}^2(\zeta)}{4\pi} \propto G(\phi(\zeta))^{-1}. \tag{15}$$

It is necessary to identify the nature of $G(\phi(\zeta))$ in order to compute $\alpha_s^{AdS}(Q^2)$ and $\beta(Q^2)$. The form of $G(\phi(\zeta))$ has been proposed in [105] and used in investigating the phenomenon of (de)confinement of glueballs. As we have demonstrated in Section 3.1, the dimensionless $G(\phi(\zeta))$ is directly associated with the tachyon potential $V(\phi)$ for strings with $T_{\rm string} = 1$ corresponding to $(2\pi\alpha')^2 = 1$ and we can express

$$V(\phi(\zeta)) = G(\phi(\zeta)) = \frac{\Lambda}{4}[\phi(\zeta)^2 - a^2]^2. \tag{16}$$

We will use this function to induce confinement and deconfinement transitions. In the string-theory normalization $(2\pi\alpha')^2 = 1$ [35] (see below Equation (11)), the tachyon field ϕ is dimensionless [113,124]. Consequently, in the potential given in Equation (16), the parameters Λ and a are dimensionless constants. With the linear ansatz $\phi(z) = \alpha z$, the parameter α has dimensions of energy (since z has dimensions of energy^{-1}), and the tachyon decay constant is $f_\alpha = 1/\alpha$ (with dimensions of energy^{-1}). The function $G(\phi(\zeta))$ is also dimen-

sionless, as required. The linear ansatz $\phi(z) = \alpha z$ [25–28] is the simplest deformation that preserves the AdS geometry at $z \to 0$ and introduces a single scale α (the tachyon decay constant). Motivated by the soft-wall model [29,30,50], it captures the UV behavior to leading order and describes the transition region up to a few GeV, consistent with the g_1 effective charge [37–41]. More refined profiles reproducing full pQCD running could be explored in future work, beyond this leading-order study. Therefore,

$$G(\phi) = \frac{\Lambda}{4}[(\zeta\alpha)^2 - a^2]^2. \tag{17}$$

The scale anomaly in QCD induces a nonvanishing energy-momentum trace tensor, given as

$$\left\langle \Theta^\mu_\mu \right\rangle = -\frac{9}{8}\left\langle \frac{\alpha_s}{\pi} G^{\mu\nu} G_{\mu\nu} \right\rangle, \tag{18}$$

where α_s is the strong coupling and $G^{\mu\nu}$ is the non-abelian gauge field strength. Using the parton-hadron duality principle [125–128], we can establish a relation between $\left\langle \Theta^\mu_\mu \right\rangle$ and Λ as

$$\begin{aligned} \left\langle \Theta^\mu_\mu \right\rangle &= \left(4V(\phi) - \phi\frac{dV}{d\phi}\right)\Big|_{\phi_0=0} \\ &= 4V(\phi_0) = \Lambda a^4. \end{aligned} \tag{19}$$

Equating Equations (18) and (19) yields,

$$\Lambda = \frac{9\left\langle \alpha_s G^{\mu\nu} G_{\mu\nu} \right\rangle}{8\pi a^4}; \tag{20}$$

hence, the coupling Λ, is proportional to the gluon condensate [129]. Now, calculating the physical running coupling measured on Q^2-scale, we use the Mellin transform. The Mellin transform relating the holographic coordinate ζ to momentum space follows from the AdS/CFT correspondence, where ζ is dual to the renormalization scale $\mu \sim 1/\zeta$ [130]. The bulk-to-boundary propagator for a scalar field of mass $\tilde{m}_\phi$ in AdS_5 introduces a weight $\zeta^{Q^2/|\tilde{m}_\phi^2|-1}$.

The integrand in Equation (17) contains a double pole on the real axis at $\zeta_0 = a/\alpha$, rendering the naive integral ill-defined. The physical coupling $\alpha_s^{\mathrm{AdS}}(Q^2)$ is therefore defined by analytic continuation, implemented through the prescription $\zeta \to \zeta + i\varepsilon$ with $\varepsilon \to 0^+$, which shifts the pole infinitesimally off the contour. The resulting expression is evaluated in the sense of distributions, reducing to a Cauchy principal value integral after a single integration by parts, as detailed in Appendix A. Carrying out the Mellin transform yields

$$\begin{aligned} \alpha_s^{\mathrm{AdS}}(Q^2) &\sim \int_0^\infty \alpha_s^{\mathrm{AdS}}(\zeta)\, \zeta^{Q^2/|\tilde{m}_\phi^2|-1}\, d\zeta \\ &= \frac{\sigma\pi}{\Lambda a^4 |\tilde{m}_\phi^2|}\left(-\frac{\alpha^2}{a^2}\right)^{-Q^2/2|\tilde{m}_\phi^2|} (2|\tilde{m}_\phi^2| - Q^2)\csc\left(\frac{\pi Q^2}{2|\tilde{m}_\phi^2|}\right) \\ &= \frac{\sigma\Lambda\pi}{|\tilde{m}_\phi^6|}\left(\frac{|\tilde{m}_\phi^2|}{\Lambda} f_\alpha^2\right)^{Q^2/2|\tilde{m}_\phi^2|} (2|\tilde{m}_\phi^2| - Q^2)\csc\left(\frac{\pi Q^2}{2|\tilde{m}_\phi^2|}\right). \end{aligned} \tag{21}$$

The trigonometric structure arises from the Euler reflection formula $\Gamma(p)\Gamma(1-p) = \pi/\sin(\pi p)$ underlying the Mellin transform of functions with poles on the integration contour. In particular, the cosecant factor emerges from the principal value integral after combining contributions at shifted arguments, as shown in Appendix A. To avoid ambiguity between UV and IR mass scales, we distinguish the tachyonic instability scale

at the false vacuum from the physical glueball mass. At $\phi = 0$, the potential curvature defines $\tilde{m}_\phi^2 = V''(0) = -\Lambda a^2 < 0$, which characterizes the UV deformation. Since a tachyon has spacelike momentum, $p^2 = \tilde{m}_\phi^2 < 0$, physical observables depend only on its magnitude. We therefore define the positive scale $m_{\phi,\mathrm{UV}}^2 \equiv |\tilde{m}_\phi^2| = \Lambda a^2$, which enters the running coupling. This is required to keep the Mellin representation (Equation (21)) real, as using $\tilde{m}_\phi^2 < 0$ would lead to an unphysical complex coupling. In contrast, the physical glueball mass arises from fluctuations about the true vacuum $\phi = \pm a$, where $m_\phi^2 = V''(\pm a) = 2\Lambda a^2 > 0$ (which will be discussed in detail in Section 5). The two scales are related by $m_\phi = \sqrt{2}\,|\tilde{m}_\phi|$. Numerically, we take $|\tilde{m}_\phi| = 0.86$ GeV and $m_\phi = 1.73$ GeV as independent lattice-informed inputs, with their ratio consistent with the model expectation at leading order.

We substituted (Equation (15)) and divided Q^2 by $|\tilde{m}_\phi^2|$ in the integral for dimensional consistency. We will demonstrate below that the mass scale is related to the scale Q_Λ at which pQCD breaks down in the model framework. The constant σ originates from the string tension, $T_{\mathrm{string}} = 1/(2\pi\alpha')$ and $\sigma = T_{\mathrm{string}}^2$, where T_{string} is the Dp-brane string tension. In string units where $(2\pi\alpha')^2 = 1$, all dimensionful quantities are measured in terms of the string energy scale $E_s = 1/\sqrt{\alpha'} = \sqrt{2\pi}$ (in units of the string length), so that $\sigma = T_{\mathrm{string}}^2 = 1/(2\pi\alpha')^2 = 1$ is consistent. Upon restoring physical units, one identifies E_s with a physical mass scale; since the only explicit scale in Equation (21) is $|\tilde{m}_\phi|$, we set $E_s \equiv |\tilde{m}_\phi|$, which yields $\sigma = E_s^4 = |\tilde{m}_\phi^4|$ in GeV^4.

We showed in (Equation (11)) and stated below it that $G(\phi)$ is a dimensionless function associated with the tachyon potential through the Regge slope, so the proportionality constant serves as a dimensional correction to the expression since dimensionful quantities such as the glueball mass and the energy scale Q^2 were introduced. It should be noted that in the tachyon potential, a and ϕ have dimensions of energy, but $G(\phi)$ is dimensionless. For mathematical convenience, we set the dimensionless coupling constant, Λ, to unity, $\Lambda = 1$, and also recall $\sigma = |\tilde{m}_\phi^4|$ for dimensional consistency. Therefore, Equation (21) simplifies to

$$\alpha_s^{AdS}(Q^2) = \frac{\sigma\pi}{|\tilde{m}_\phi^6|}\left(|\tilde{m}_\phi^2| f_\alpha^2\right)^{Q^2/2|\tilde{m}_\phi^2|}(2|\tilde{m}_\phi^2| - Q^2)\csc\left(\frac{\pi Q^2}{2|\tilde{m}_\phi^2|}\right). \tag{22}$$

We emphasize that Equation (22) applies in the regime $Q^2 \lesssim |\tilde{m}_\phi^2|$. For $Q^2 \to \infty$, it falls as $1/Q^2$, characteristic of a tree-level bulk result. The logarithmic running of perturbative QCD would require quantum corrections in the bulk or a running tachyon profile $\phi(z)$. Thus, the model describes the IR–intermediate regime, while the deep UV requires additional physics, such as the dynamically generated gluon mass introduced in Section 6.1.

We plot the leading order of the perturbative result of the QCD running coupling given by

$$\alpha_s^{pQCD}(Q^2) = \frac{4\pi}{\beta_0 \ln\left(\dfrac{Q^2}{\Lambda_{QCD}^2}\right)} \tag{23}$$

where Λ_{QCD} is the QCD scale,

$$\beta_0 = 11 - \frac{2}{3}n_f, \tag{24}$$

is the first term of the β-series, with n_f the number of quark flavors active at scale Q^2.

4.2. Beta-Function

The β-function is calculated using the renormalization group theory,

$$\begin{aligned}\beta\Big(\alpha^{\mathrm{AdS}}(Q^2)\Big) &= \frac{d\,\alpha^{\mathrm{AdS}}(Q^2)}{d\ln Q^2}\\ &= -\frac{Q^2\pi\sigma}{2|\tilde{m}_\phi^8|}\left(f_\alpha^2|\tilde{m}_\phi^2|\right)^{\frac{Q^2}{2|\tilde{m}_\phi^2|}}\csc\left(\frac{\pi Q^2}{2|\tilde{m}_\phi^2|}\right)\Bigg[(2|\tilde{m}_\phi^2|-Q^2)\left(\pi\cot\left(\frac{\pi Q^2}{2|\tilde{m}_\phi^2|}\right)\right.\\ &\qquad\left.-\log\left(f_\alpha^2|\tilde{m}_\phi^2|\right)\right)+2|\tilde{m}_\phi^2|\Bigg].\end{aligned} \tag{25}$$

The β-function follows from differentiating Equation (22). It inherits the poles of $\alpha_s^{\mathrm{AdS}}(Q^2)$ (see Figure 1) at $Q^2 = 2n\tilde{m}_\phi^2$, where n is an integer, but remains well defined and negative below the first pole ($Q^2 < 2|\tilde{m}_\phi^2|$), satisfying asymptotic freedom. In QCD, the β-function vanishes in both the UV (asymptotic freedom) and IR [131] (conformal fixed-point [132]) limits, reflecting the decoupling of colored degrees of freedom in the infrared [54]. The other condition is,

$$\beta(Q) < 0 \qquad \text{for} \qquad Q > 0. \tag{26}$$

This condition reflects the anti-screening behavior of the QCD theory at large Q, where its running coupling, α_s, vanishes due to asymptotic freedom with quark-gluon degrees of freedom. The QCD β-function is generally negative, and its value increases from the UV regime and assumes its maximum value in the IR domain.

We expect the β-function to have a usual analytical behavior in both the UV and the IR regimes with or without the Landau pole in α_s. The 'usual' behavior of $\beta(Q^2)$ is due to its conformal invariant characteristics, leading to the well-behaved cut-off in both the IR and the UV regimes, regardless of the singularity exhibited by α_s.

The result in Equation (22) displays the expected decrease in α_s at large Q^2 similar to the running coupling displayed for pQCD in Figure 2. We determine the position of the Landau pole Q_Λ in Equation (22) using the relation for determining the transition point,

$$\frac{d\beta}{dQ} = 0. \tag{27}$$

However, the results obtained from the above operation are not analytically solvable for Q_Λ because of the trigonometric functions involved. So, we expand it for a small Q, leading to

$$\frac{8}{|\tilde{m}_\phi^2|Q^3} + \frac{\left(\pi^2 - 3\log[f_\alpha^2|\tilde{m}_\phi^2|]\right)Q}{3|\tilde{m}_\phi^6|} + \mathcal{O}(Q)^3 = 0. \tag{28}$$

This result yields,

$$Q_\Lambda = \left(\frac{24}{-\pi^2 + \log[f_\alpha^2\tilde{m}_\phi^2]}\right)^{1/4}\tilde{m}_\phi. \tag{29}$$

The apparent singularity from $\csc(\pi Q^2/(2|\tilde{m}_\phi^2|))$ at $Q^2 = 2|\tilde{m}_\phi^2|$ is canceled by the factor $(2|\tilde{m}_\phi^2| - Q^2)$; so, the actual Landau pole must be determined from the full expression, e.g., via $d\beta/dQ = 0$. Expanding this equation in the small parameter $Q/|\tilde{m}_\phi|$ (the relevant dimensionless ratio) gives the polynomial Equation (28). Although $Q_\Lambda/|\tilde{m}_\phi| \approx 0.67$ is not negligible, $(Q_\Lambda/|\tilde{m}_\phi|)^2 \approx 0.45 < 1$, suppressing higher-order terms and making the first nonvanishing approximation reliable. The resulting Q_Λ also agrees with the QCD scale from pQCD matching in Figure 2, supporting the estimate. Using the parameters from Figures 1–3, $|\tilde{m}_\phi| = 0.86$ GeV and $f_\alpha = 0.50\ \mathrm{GeV}^{-1}$, we find $Q_\Lambda \approx 0.58$ GeV for the Landau pole, indicated by a solid blue line in those figures. This singularity marks the scale

where pQCD breaks down and is often associated with the confinement or hadronic scale. It also reflects the scale dependence of α_s and serves as an expansion parameter for related quantities such as the β-function [52]. The tachyon decay constant $f_\alpha = 1/\alpha = 0.50\ \text{GeV}^{-1}$ sets the scale of the tachyon field in the holographic direction. It is chosen so that the model's Landau pole Q_Λ aligns with the QCD scale $\Lambda_{\text{QCD}} \approx 0.58$ GeV, ensuring a smooth UV–IR transition (Figure 2). To verify the reliability of the expansion, we numerically solved the full condition $d\beta/dQ = 0$ using the exact expression for $\beta(Q)$ (Equation (25)). With the parameters $|\tilde{m}_\phi| = 0.86$ GeV and $f_\alpha = 0.50\ \text{GeV}^{-1}$, the root is found at $Q_\Lambda = 0.58273$ GeV, in excellent agreement with the approximate value 0.58 GeV. This confirms the validity of the truncated expansion.

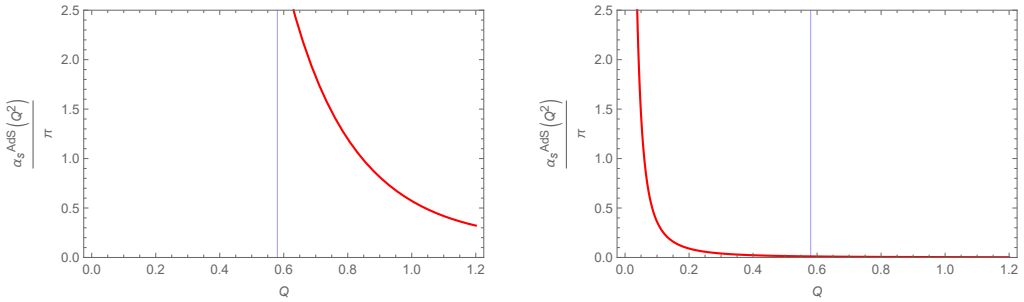

(**a**) Left Panel (**b**) Right Panel

Figure 1. A graph of $\alpha_s^{AdS}(Q^2)/\pi$ against Q for $|\tilde{m}_\phi| = 0.86\,\text{GeV}$ (**a**) and $|\tilde{m}_\phi| \to \infty$ (**b**). We compare the graph (**a**) with the ones contained in Refs. [29,50] for $\alpha_{g1}(Q)/\pi$ (pQCD) and other experimental data in [133], and we observe the expected decrease in α_s at large Q. We present results for both the lightest glueball mass (**a**) and the heaviest possible glueball mass (**b**). However, the theory governing the study is consistent with light glueball masses, so the graph in the right panel is for analytical purposes and may not have any physical implications. We observe that $\alpha_s^{AdS}(Q^2)$ decreases sharply with increasing Q; on the other hand, an increase in $|\tilde{m}_\phi| \to \infty$ moves the graph more towards a small Q region beyond the Landau pole, Q_Λ, (vertical blue line) and also falls quickly at large Q. Thus, heavy glueballs are more likely to be tightly bound than lighter ones.

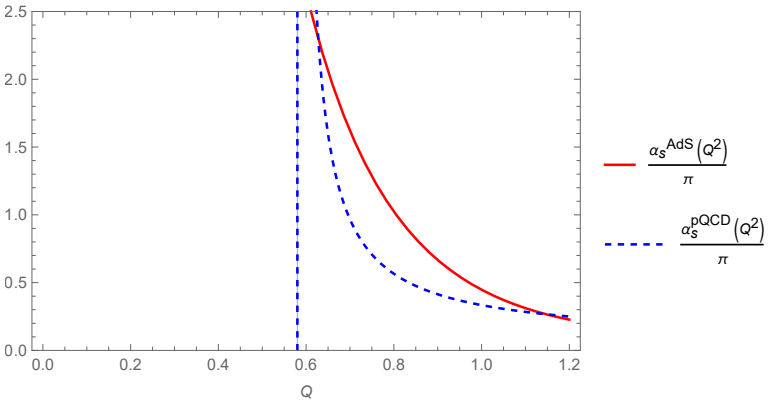

Figure 2. Comparison of the running coupling from the UV deformation (red solid line) with the leading-order pQCD result (blue dashed line) for pure gluon states ($n_f = 0$). The Landau poles are matched at $\Lambda_{\text{QCD}} = 0.58\,\text{GeV}$ (vertical lines). The model shows a power-law falloff, whereas pQCD exhibits logarithmic running; this difference is expected, as the UV deformation describes the intermediate energy regime where the transition from nonperturbative to perturbative dynamics occurs. Reproducing the asymptotic logarithmic behavior would require bulk quantum corrections beyond this leading-order holographic framework.

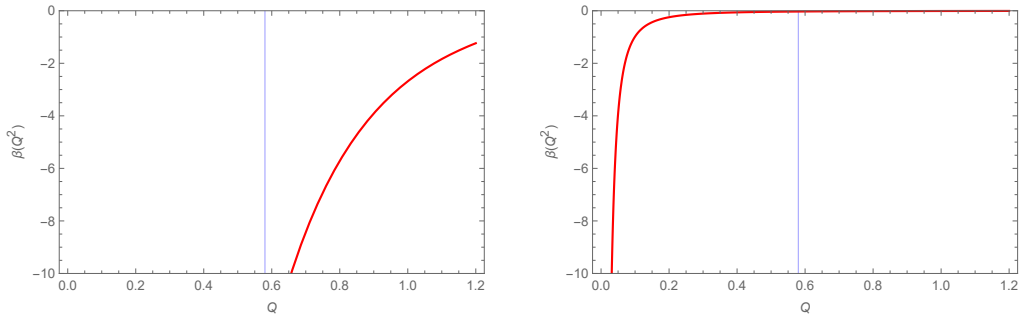

(**a**) Left Panel (**b**) Right Panel

Figure 3. A graph of $\beta(Q^2)$ against Q for $|\tilde{m}_\phi| = 0.86\,\text{GeV}$ (**a**) and $|\tilde{m}_\phi| \to \infty$ (**b**). The graph (**a**) is compared with $\beta(Q)$ (pQCD) reproduced in Refs. [29,62]. The graph in the right panel shows the behavior of the $\beta(Q^2)$ for $|\tilde{m}_\phi| \to \infty$.

5. Deformation of the AdS Space in the IR Regime

For the nonperturbative behavior of couplings, we perturb the tachyon fields about their 'true' vacuum $\phi_0 = \pm a$ by introducing a new field η through $\phi \to \eta + \phi_0$. This stabilizes the tachyons and the new field acquires a positive mass $V''(\phi)|_{\phi_0=\pm a} = 2a^2\Lambda = m_\phi^2$. Consequently, Equation (16) becomes

$$\begin{aligned} V(\eta) &= V(\phi)\big|_{\phi_0} + V'(\phi)\big|_{\phi_0}\eta + \frac{1}{2}V''(\phi)\big|_{\phi_0}\eta^2 \\ &= \frac{1}{2}m_\phi^2\eta^2. \end{aligned} \tag{30}$$

This process coincides with *tachyon condensation*. The new field η is identified with a stable glueball field [105] in the IR regime with a solution

$$\eta(\zeta) = \frac{e^{m_\phi\zeta}}{\zeta}, \tag{31}$$

which produces confinement of glueballs in the limit of large particle separation distance, where *color confinement* is expected. The solution, $\eta(\zeta)$, is obtained by including the kinetic term $\frac{1}{2}(\partial_\mu\phi)^2$ of the tachyonic field in the action (presented in Equation (11)) and expanding around the true vacuum $\phi_0 = \pm a$ with the shift $\phi = \phi_0 + \eta$ [34]. The linearized equation of motion in spherical coordinates is given by:

$$\Big[-\frac{d^2}{d\zeta^2} + \frac{2}{\zeta^2} + V''(\phi_0)\Big]\eta(\zeta) = 0,$$

with $m_\phi^2 = V''(\pm a) = 2\Lambda a^2$, which corresponds to the physical scalar glueball mass. This procedure follows the standard holographic treatment of scalar fields in AdS [1,2,6,134] and is consistent with the AdS/CFT dictionary [1,3]. A comprehensive study can be found in our previous papers [31–34], further establishing that in the limit, $r \to \infty$, this solution is dominant.

5.1. Strong Running Coupling

Using the *color dielectric function* for the condensed tachyons, Equation (15) alters to

$$\alpha_s^{AdS}(\zeta) \propto G(\eta(\zeta))^{-1}. \tag{32}$$

Using the Laplace transform

$$\alpha_s^{AdS}(Q^2) \sim \int_0^\infty \alpha_s^{AdS}(\zeta) e^{-Q^2\zeta/m_\phi} d\zeta = \frac{4m_\phi \rho}{(2m_\phi^2 + Q^2)^3}, \tag{33}$$

where ρ is a proportionality constant. At $Q = 0$, $\rho = 2m_\phi^5 \alpha_s^{AdS}(0)$, and the above expression transforms into

$$\alpha_s^{AdS}(Q^2) = \frac{(2m_\phi^2)^3}{(2m_\phi^2 + Q^2)^3} \alpha_s^{AdS}(0). \tag{34}$$

The condensed phase $\eta(\zeta)$ yields a confining background. The color dielectric function $G(\eta)$ produces a linear confining potential (area law) [135] and a mass gap m_ϕ [105,136]. By contrast, the UV phase with free tachyons corresponds to a deconfined, perturbative regime (discussed in Section 4). Thus, the model provides a clear distinction between confining and non-confining scenarios through the vacuum expectation value of the tachyon field.

5.2. Beta-Function

We can also calculate the β-function from Equation (25), which leads to the expression

$$\beta(Q^2) = -\frac{3(2m_\phi^2)^3 Q^2}{(2m_\phi^2 + Q^2)^4} \alpha_s^{AdS}(0). \tag{35}$$

This expression satisfies the restrictions

$$\beta(Q \to 0) = \beta(Q \to \infty) = 0 \quad \text{and} \quad \beta(Q) < 0 \quad \text{for} \quad Q > 0. \tag{36}$$

The first condition satisfies the restrictions that QCD approximates conformal theory in both the far UV and the deep IR regimes, known as "the principle of maximum conformality"; meanwhile, the second condition is a consequence of the asymptotic freedom properties of QCD theory. Hence, $\alpha_s^{AdS}(Q^2)$ can be normalized to α_{s,g_1} (see Figure 4 above), a well-measured effective charge obtained from the Bjorken sum rule [38] for polarized deep inelastic lepton-proton scattering, by exploring the similarities in the qualitative behavior of the β-functions. It vanishes in the deep infrared domain, rises to a higher negative immediately, and falls off to zero in the far UV domain. We take advantage of these similar features and normalize $\alpha_s^{AdS}(Q^2 = 0) = \pi$ for comparison. Taking the derivative with respect to Q

$$\frac{d\beta}{dQ} = -\frac{6(2m_\phi^2)^3 Q\pi}{(2m_\phi^2 + Q^2)^4} \left[1 - \frac{4Q^2}{2m_\phi^2 + Q^2}\right]; \tag{37}$$

consequently, there is a transition at $Q_0 = \sqrt{(2/3)} m_\phi$. Perturbation theory is applicable in the regime $Q_0 > \sqrt{(2/3)} m_\phi$, whilst non-perturbation theory is applicable in the regime $Q_0 < \sqrt{(2/3)} m_\phi$. Also, the conditions

$$\left.\frac{d\beta}{dQ}\right|_{Q=Q_0} = 0, \qquad \left.\frac{d\beta}{dQ}\right|_{Q_0} < 0 \quad \text{for} \quad Q < Q_0 \quad \text{and} \quad \left.\frac{d\beta}{dQ}\right|_{Q_0} > 0 \quad \text{for} \quad Q > Q_0 \tag{38}$$

are all satisfied [29,30].

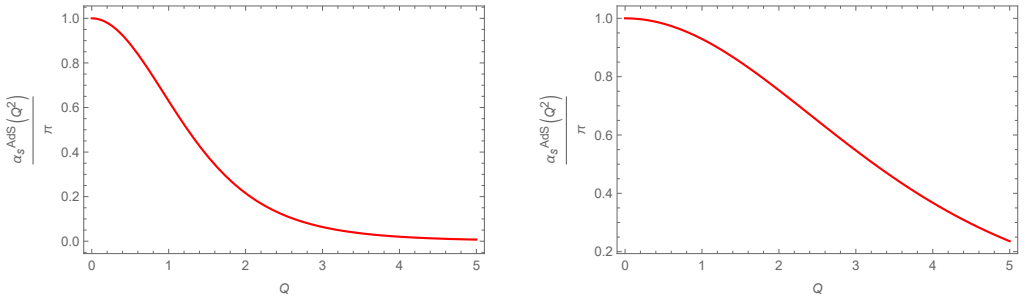

(**a**) Left Panel (**b**) Right Panel

Figure 4. (**a**): $\alpha_s^{\mathrm{AdS}}(Q^2)/\pi$ as a function of Q for the physical glueball mass $m_\phi = 1.73\,\mathrm{GeV}$ (from lattice QCD). The solid red curve is compared with the effective charge $\alpha_{s,g1}(Q)$ extracted from the Bjorken sum rule (data points from Refs. [29,50,62]), normalized such that $\alpha_s^{\mathrm{AdS}}(0) = \pi$. All model parameters are fixed by independent lattice and QCD inputs (see Sections 4 and 5), so the agreement constitutes a genuine test of the framework. (**b**): the same coupling in the limiting case $m_\phi \to \infty$ (artificially heavy glueballs), illustrating that increasing m_ϕ leads to stronger binding, as expected within the model.

6. Analysis and Conclusions

6.1. Analysis

The graphs plotted for the couplings determined from the UV region were for $f_\alpha = 0.50\,\mathrm{GeV}$ and $|\tilde{m}_\phi| = 0.86\,\mathrm{GeV}$, both determined via the Landau pole condition. The glueball mass m_ϕ is fixed by the tachyon potential: expanding around $\phi_0 = \pm a$ gives m_ϕ^2. We calibrate it to match the lattice QCD value $m_\phi = 1.73$ GeV, preserving the model's predictive power. Generally, we considered the *lightest scalar glueball mass* consistent with the background of the study presented in Section 3. From QCD lattice simulations results, QCD sum rule, and QCD phenomenology, the *lightest scalar glueball mass* with quantum number $J^{PC} = 0^{++}$ and frequency $f_0(1710)$, has been determined to be $m_\phi = 1.73\,\mathrm{GeV}$ [32–34] (and references therein). Other glueball masses with the same quantum number and frequencies $f_0(500)$, $f_0(980)$, $f_0(1370)$ have also been identified [137,138]. Figure 5 shows how the transition point between the two regimes, marked by $\beta(Q^2)$, depends on the magnitude of m_ϕ.

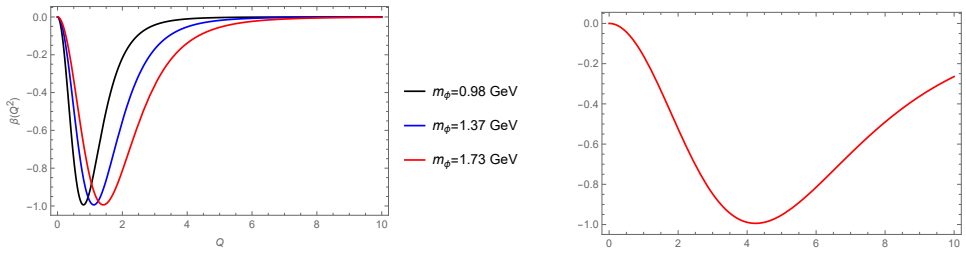

(**a**) Left Panel (**b**) Right Panel

Figure 5. (**a**): $\beta(Q^2)$ as a function of Q for three glueball masses m_ϕ (colored curves). All parameters are fixed by independent lattice inputs (see Sections 4 and 5). The transition momentum $Q_0 = 2/3\, m_\phi$ marks the minimum of $\beta(Q)$: for $m_\phi = 1.73$ GeV (red), $Q_0 \approx 1.41$ GeV; for $m_\phi = 1.37$ GeV (black), $Q_0 \approx 1.12$ GeV; for $m_\phi = 0.98$ GeV (blue), $Q_0 \approx 0.80$ GeV. The curves are compared with the AdS/QCD and modified AdS/QCD β-functions from Refs. [29,62], showing better agreement with the modified AdS case. For $Q > Q_0$, $\beta(Q)$ remains negative, reflecting asymptotic freedom. (**b**): the limiting case $m_\phi \to \infty$ (all curves collapse to the same shape) illustrates that heavier glueballs shift the transition to larger momenta, consistent with the scaling $Q_0 \propto m_\phi$.

We emphasize that the expression in Equation (22) is valid for $Q^2 < 2|\tilde{m}_\phi^2|$, where it remains real and well defined. In our analysis, the Landau pole at $Q_\Lambda \approx 0.58\,\mathrm{GeV}$ lies well

below the threshold $Q \approx \sqrt{2}\,|\tilde{m}_\phi| \approx 1.22\,\text{GeV}$, so the model applies to the intermediate energy region rather than the asymptotic UV. For $Q^2 \gg 2|\tilde{m}_\phi^2|$, the expression develops poles and ceases to be physical. At large Q^2, Equation (22) exhibits a power-law (exponential) falloff, not the logarithmic running of pQCD, confirming that the UV deformation captures the transition from the IR to intermediate scales. Reproducing asymptotic behavior would require bulk quantum corrections beyond this leading-order framework.

We established the connection between the couplings ($\alpha_s^{\text{AdS}}(Q^2)$ and $\beta(Q^2)$) and the mass scales m_ϕ and $\tilde{m}_\phi$ in the IR and UV regions, respectively. The Landau pole is located at $Q_\Lambda \approx 0.58$ GeV (Equation (29)), related to the UV mass scale, while the transition momentum in the IR is $Q_0 = \sqrt{2/3}\,m_\phi$, giving $Q_0 \approx 1.41$ GeV for $m_\phi = 1.73$ GeV. This indicates that heavier glueballs are more tightly bound, analogous to the behavior of heavy quarks. The UV mass scale $|\tilde{m}_\phi| = 0.86$ GeV and the IR glueball mass $m_\phi = 1.73$ GeV both arise from the tachyon potential Equation (16). Expansions about the false and true vacua give $\tilde{m}_\phi^2 = -\Lambda a^2$ and $m_\phi^2 = 2\Lambda a^2$, respectively, implying $m_\phi = \sqrt{2}\,|\tilde{m}_\phi|$, analogous to connections between the scalar glueball mass and the gluon condensate found in QCD effective models [139]. While the lattice value $m_\phi = 1.73$ GeV predicts $|\tilde{m}_\phi| \approx 1.22$ GeV, we fix $|\tilde{m}_\phi| = 0.86$ GeV phenomenologically by matching the Landau pole to Λ_{QCD}, with the $\sim$30% deviation consistent with leading-order accuracy. The transition scale $Q_0 \approx 0.89$ GeV (Figure 6) then emerges as the intersection of the UV and IR couplings.

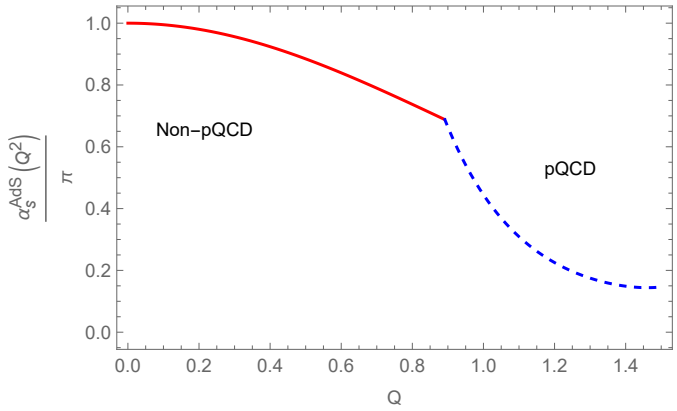

Figure 6. A unified diagram for $\alpha_s^{AdS}(Q^2)$ in both the IR (non-pQCD) and the UV (pQCD) regions. A schematic diagram showing the behavior of the strong running coupling in both the UV (dashed blue) and IR (red) regions in the model framework. This diagram shows the transition point at 0.89 GeV (the two graphs Figure 1a and Figure 4b intersect at this point), corresponding to $m_\phi \approx 1.09$ GeV.

The power-law falloff in Equation (34) characterizes the confining phase and describes the coupling in the infrared and intermediate momentum regions (up to a few GeV), remaining finite at $Q = 0$. It does not reproduce the asymptotic logarithmic running of pQCD, which occurs in the deep UV and is governed by the free-tachyon deformation with its unphysical pole at $Q = 0$ (Section 4.1). Together, the IR and UV sectors provide a unified description across scales, with the transition near $Q_0 \sim 0.89$ GeV (Figure 6).

This paper presents a new approach to determining the AdS/QCD running coupling and associated β-function. Rather than fixing $\alpha_s^{AdS}(Q^2)$ in the poorly understood IR and extrapolating to the UV, we introduce a tachyon-induced function $G(\phi)$ that deforms AdS space differently in the free (UV) and condensed (IR) regimes. The resulting couplings are compared with the effective charge $\alpha_{s,g1}$ from the Bjorken sum rule.

In the UV, we obtain a sinusoidal behavior, $\alpha_s^{AdS}(Q^2) \sim 1/\sin(\pi Q^2/2|\tilde{m}_\phi^2|)$, in contrast to the logarithmic pQCD running $\alpha_s(Q^2) \sim 1/\ln(Q^2/\Lambda^2_{\text{QCD}})$. In the IR, instead of the exponential soft-wall result $\alpha_s^{AdS}(Q^2) \sim e^{-Q^2/4\kappa^2}$, our model yields a power-law

falloff $\alpha_s^{AdS}(Q^2) \sim 1/(2|\tilde{m}_\phi^2| + Q^2)^3$ (see Figure 4). Given that the IR behavior of the QCD coupling is not uniquely determined experimentally [40,133], hadronic observables remain the most reliable benchmarks for comparison with lattice results [140]. Finally, the derived β-functions satisfy the principle of maximum conformality in both UV and IR regimes.

The UV deformation of AdS space (Section 4) leads to a nonphysical *Landau singularity* in $\alpha_s^{AdS}(Q^2)$ at Q_Λ, signaling the breakdown of perturbative QCD. In contrast, the IR deformation (Section 5) yields a regular coupling in both the deep IR and far UV, consistent with the expected *IR freezing*. Experimental [141] and lattice [142] results support a finite coupling across all scales, motivating mechanisms that remove the Landau pole and IR renormalons [143] and ensure finite Q.

At low energies ($Q^2 \to 0$), gluons are expected to acquire a dynamical mass, $Q^2 = -q^2 \cong m_A^2$ [144–147], which regulates the IR behavior and leads to a finite coupling. Introducing m_A^2 into Q^2 preserves the UV limit while dominating in the IR, thereby defining an *IR freezing point* [131,148–151] and improving the description of confinement. This dynamically generated gluon mass is unrelated to chiral symmetry breaking; instead, it reflects strong gluon interactions that form bound states such as scalar ($J^{PC} = 0^{++}$) glueballs, associated with the gluon condensate $\langle G^{\mu\nu} G_{\mu\nu} \rangle$.

In this context, the gluon mass can be related to the scalar glueball mass. For instance, leading-order Yang–Mills analyses with an auxiliary field ϕ give $m_A = m(0^{++})/\sqrt{6}$ [139,152], while color dielectric models yield $m_A = m_\phi/2$ [33,34]. Accordingly, $\alpha_s^{AdS}(Q^2)$ in the UV region takes the form

$$\alpha_s^{AdS}(Q^2 + m_A^2) = \frac{\sigma\pi}{|\tilde{m}_\phi^6|}\left(|\tilde{m}_\phi^2| f_\alpha^2\right)^{(Q^2+m_A^2)/2|\tilde{m}_\phi^2|}(2|\tilde{m}_\phi^2| - (Q^2 + m_A^2))\csc\left(\frac{\pi(Q^2 + m_A^2)}{2|\tilde{m}_\phi^2|}\right). \tag{39}$$

For $|\tilde{m}_\phi| = 0.86$, we get $m_A = 0.43$, which leads to a finite IR freezing point, as presented in Figures 7 and 8. On the other hand, the IR model self-regulates at low Q^2 with a finite freezing point normalized at $\alpha_s^{AdS}(0) = \pi$, on g_1 scheme [50].

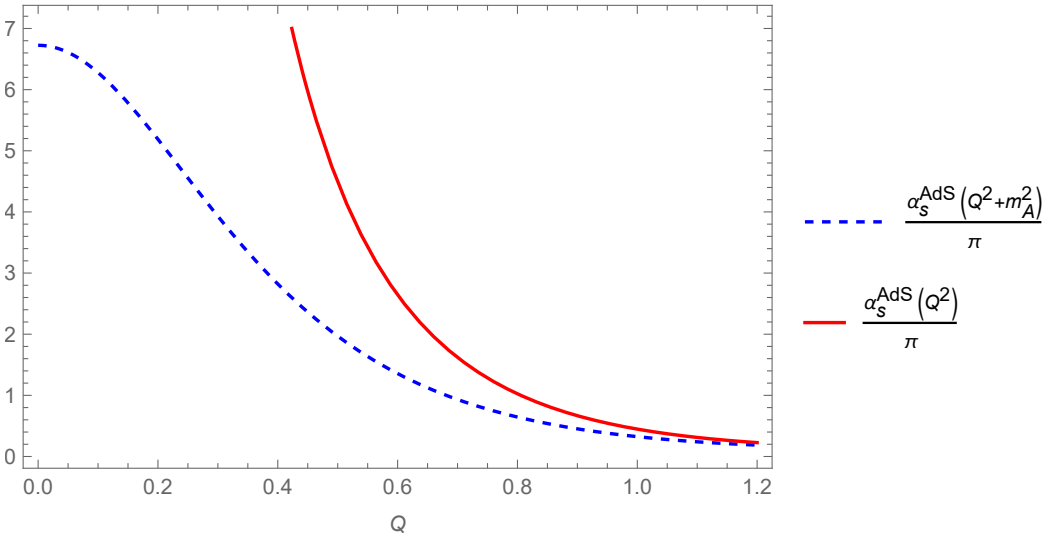

Figure 7. A graph of $\alpha_s^{AdS}(Q^2 + m_A^2)/\pi$ (dashed blue) and $\alpha_s^{AdS}(Q^2)/\pi$ (red) against Q for $m_A = 0.43\,\text{GeV}$ and $|\tilde{m}_\phi| = 0.86\,\text{GeV}$. The dashed blue graph is well behaved in the IR region due to the IR freezing point, while the red graph shows the singularity in the UV region. However, in the limit of high Q, they both fall off in a similar manner.

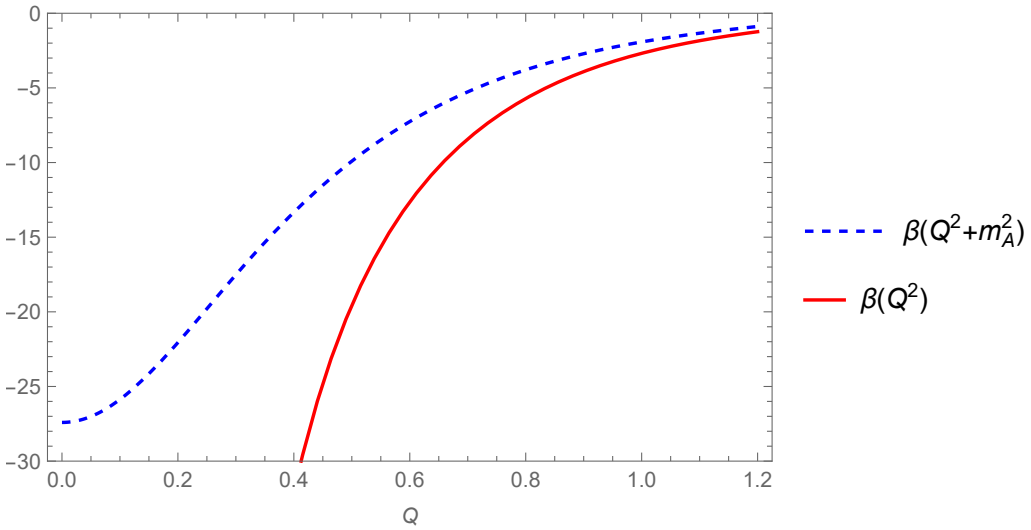

Figure 8. A graph of $\beta(Q^2 + m_A^2)$ (dashed blue) and $\beta(Q^2)$ (red) against Q for $m_A = 0.43\,\text{GeV}$ and $|\tilde{m}_\phi| = 0.86\,\text{GeV}$. We compare the β-function with IR freezing to the one without IR freezing.

6.2. Conclusions

In this work, we constructed the tachyonic AdS/QCD action from the DBI action and studied the running coupling $\alpha_s^{AdS}(Q^2)$ and its associated $\beta(Q^2)$ by distorting the AdS_5 background through tachyon-induced color dielectric functions. We showed that free tachyons deform the AdS space in the UV region, reproducing qualitative features consistent with perturbative QCD and the $\alpha s, g1$ effective charge, while condensed tachyons dominate in the IR, yielding behavior characteristic of nonperturbative QCD. Increasing the glueball mass m_ϕ enhances color confinement and raises the transition momentum, with heavier glueballs confining more strongly than lighter ones.

We further provided a unified description of $\alpha_s^{AdS}(Q^2)$ across UV and IR scales, identifying a transition at $Q_0 \sim 0.89\,\text{GeV}$, corresponding to $m_\phi \approx 1.09\,\text{GeV}$. A Landau singularity was observed in the UV, which we resolved by introducing a dynamically generated gluon mass, thereby correcting the unphysical $Q \to 0$ limit. Overall, our framework establishes a consistent relation between $\alpha_s^{AdS}(Q^2)$, $\beta(Q^2)$, and m_ϕ ($|\tilde{m}_\phi|$), showing that suitable tachyon potentials, particularly of Higgs-like form, allow the AdS background to capture both perturbative and nonperturbative QCD dynamics within a unified approach.

The framework developed in this work opens several promising directions for future investigation. The use of a tachyon-induced color dielectric function to deform the gravitational background is not restricted to the AdS/QCD context considered here. It would be of particular interest to extend this mechanism to other gauge/gravity dualities, including non-supersymmetric AdS/CFT scenarios, to study confinement–deconfinement transitions in a broader setting. Additionally, exploring a possible AdS/electroweak correspondence may offer new insights into the running of the electroweak coupling and mass generation, in analogy with the holographic role played by the tachyon in this model. Finally, a direct phenomenological application of the present framework lies in fitting the glueball-mediated potential derived here to heavy quarkonium spectroscopy, which would allow a quantitative assessment of glueball contributions to quark confinement across different mass scales.

Author Contributions: Conceptualization, A.I., E.A.A. and F.A.B.; Methodology, A.I., E.A.A. and F.A.B.; Validation, F.A.B.; Formal analysis, A.I., E.A.A. and F.A.B.; Investigation, A.I., E.A.A. and F.A.B.; Writing—original draft, A.I. and F.A.B.; Writing—review and editing, A.I., E.A.A. and F.A.B.; Supervision, F.A.B.; Project administration, F.A.B. All authors have read and agreed to the published version of the manuscript.

Funding: This work is partially supported by Conselho Nacional de Desenvolvimento Científico e Tecnológico (CNPq) project No.: 168546/2021-3, Brazil. A. I. and E. A. A. acknowledge financial support from the São Paulo State Research Foundation (FAPESP), Grants No. 2023/09545-1, 2025/17347-0, and 2024/05377-0. F. A. B. acknowledges support from CNPq (Grant No. 309092/2022-1).

Data Availability Statement: The original contributions presented in this study are included in the article . Further enquiries can be directed to the corresponding author.

Acknowledgments: We thank the administrative and technical support from our institutions during the production of this study.

Conflicts of Interest: The authors declare no conflict of interest.

Glossary of Abbreviations and Terms

QCD	Quantum Chromodynamics, the fundamental theory describing strong interactions among quarks and gluons.
pQCD	Perturbative QCD, the high-energy expansion of QCD valid at short distances.
UV	Ultraviolet; high-energy or short-distance regime.
IR	Infrared; low-energy or long-distance regime.
Λ_{QCD}	QCD scale parameter separating perturbative and nonperturbative regimes.
YM Theory	Yang–Mills gauge theory underlying QCD.
LF	Light-front formulation of relativistic dynamics on surfaces defined by $x^+ = x^0 + x^3$.
LFWF	Light-front wavefunction representing the quantum state of a hadron.
Holography and String Theory	
AdS	Anti-de Sitter spacetime with constant negative curvature.
CFT	Conformal Field Theory; a quantum field theory invariant under conformal transformations.
AdS/CFT	Duality between string/gravity theory in AdS space and a CFT on its boundary.
AdS/QCD	Application of AdS/CFT techniques to model QCD phenomena.
SYM Theory	Supersymmetric Yang–Mills theory, e.g., $\mathcal{N} = 4$ SYM in holography.
DBI Action	Dirac–Born–Infeld action describing D-brane dynamics.
Dp-brane	p-dimensional object in string theory where open strings can end.
IIB String Theory	One of the two ten-dimensional supersymmetric superstring theories.
Model-Specific Quantities	
Color dielectric function $G(\phi)$	Dimensionless function induced by the tachyon field, used to deform the AdS geometry. Controls the behavior of the running coupling across UV and IR scales.
Light-front holography	Mapping between the AdS wave equation and the light-front Hamiltonian of QCD bound states.
Landau pole/Landau singularity	Scale at which a perturbative running coupling diverges, signaling breakdown of perturbation theory.

Appendix A. Detailed Derivation of the Mellin Transform

The running coupling is defined through the Mellin transform

$$\alpha_s^{\mathrm{AdS}}(Q^2) \propto \int_0^\infty \alpha_s^{\mathrm{AdS}}(\zeta)\, \zeta^{s-1}\, d\zeta, \qquad s \equiv \frac{Q^2}{|\tilde{m}_\phi^2|}, \tag{A1}$$

with $\alpha_s^{\mathrm{AdS}}(\zeta) \propto [(\alpha\zeta)^2 - a^2]^{-2}$. The integrand has a double pole at $\zeta_0 = a/\alpha$ on the real axis, regulated by $a^2 \to a^2 - i\varepsilon$ ($\varepsilon \to 0^+$).

Dimensionless form

Introducing $u = \zeta/\zeta_0$, so $\zeta = \zeta_0 u$, $d\zeta = \zeta_0\, du$. Then,

$$(\zeta\alpha)^2 - a^2 = \alpha^2\zeta_0^2(u^2-1) = a^2(u^2-1), \tag{A2}$$

and the integrand becomes

$$\alpha_s^{\mathrm{AdS}}(Q^2) \propto \frac{\zeta_0^s}{a^4}\, I(s), \qquad I(s) = \int_0^\infty \frac{u^{s-1}}{(u^2-1-i0^+)^2}\, du. \tag{A3}$$

Integration by parts

Write $(u^2-1)^{-2} = (u-1)^{-2}(u+1)^{-2}$ and integrate by parts with $dv = -(d/du)(u-1-i0^+)^{-1}\, du$ and $w = u^{s-1}(u+1)^{-2}$:

$$I(s) = \left[\frac{-u^{s-1}}{(u+1)^2(u-1-i0^+)}\right]_0^\infty + \int_0^\infty \frac{f'(u)}{u-1-i0^+}\, du, \qquad f(u) = \frac{u^{s-1}}{(u+1)^2}. \tag{A4}$$

The boundary term vanishes for $0 < \mathrm{Re}(s) < 2$: at $u \to \infty$, it decays as $u^{s-3} \to 0$; at $u = 0$, it vanishes as $u^{s-1} \to 0$ for $s > 0$. This range covers the entire physical domain $0 < Q^2 < 2|\tilde{m}_\phi^2|$.

Sokhotski–Plemelj decomposition

With $f'(u) = (s-1)u^{s-2}(u+1)^{-2} - 2u^{s-1}(u+1)^{-3}$, the Sokhotski–Plemelj theorem gives

$$I(s) = \mathrm{P.V.}\int_0^\infty \frac{f'(u)}{u-1}\, du + i\pi f'(1), \qquad f'(1) = \frac{s-2}{4}. \tag{A5}$$

The imaginary part $i\pi(s-2)/4$ is real-valued and nonzero for $s \neq 2$. It is discarded by the physical reality condition: $\alpha_s^{\mathrm{AdS}}(Q^2)$ is defined as the real part of the analytically continued expression, and $i\pi(s-2)/4$ is a contact term that vanishes at the boundary of the physical domain $s \to 2$ (i.e., $Q^2 \to 2|\tilde{m}_\phi^2|$) where the coupling reaches its first pole.

Partial fraction decomposition

To apply the Mellin identity to the principal value integral, decompose via partial fractions:

$$\frac{f'(u)}{u-1} = \frac{(s-1)u^{s-2}}{(u-1)(u+1)^2} - \frac{2u^{s-1}}{(u-1)(u+1)^3}. \tag{A6}$$

Using

$$\frac{1}{(u-1)(u+1)^2} = \frac{1}{4(u-1)} - \frac{1}{4(u+1)} - \frac{1}{2(u+1)^2}, \tag{A7}$$

$$\frac{1}{(u-1)(u+1)^3} = \frac{1}{8(u-1)} - \frac{1}{8(u+1)} - \frac{1}{4(u+1)^2} - \frac{1}{2(u+1)^3}, \tag{A8}$$

and the substitution $u \to 1/u$ to relate integrals over $(u+1)^{-k}$ to standard Mellin integrals, all terms reduce to combinations of $\int_0^\infty u^{q-1}/(u+1)^k\, du$, which are evaluated by $B(q, k-q) = \Gamma(q)\Gamma(k-q)/\Gamma(k)$.

Final result

Collecting all terms and applying the Euler reflection formula $\Gamma(p)\Gamma(1-p) = \pi/\sin(\pi p)$ yields

$$\text{P.V.}\int_0^\infty \frac{f'(u)}{u-1}\,du = \frac{\pi(2-s)}{4}\,\csc\!\left(\frac{\pi s}{2}\right), \tag{A9}$$

so that

$$\alpha_s^{\text{AdS}}(Q^2) \propto (2|\tilde{m}_\phi^2| - Q^2)\,\csc\!\left(\frac{\pi Q^2}{2|\tilde{m}_\phi^2|}\right), \tag{A10}$$

where the factor $(2-s) = (2|\tilde{m}_\phi^2| - Q^2)/|\tilde{m}_\phi^2|$ comes directly from the residue $f'(1) = (s-2)/4$ (via the $(u-1)^{-1}$ terms in the partial fraction decomposition) and the csc from the Euler reflection structure of the Beta function.

References

1. Gubser, S.S.; Klebanov, I.R.; Polyakov, A.M. Gauge theory correlators from noncritical string theory. *Phys. Lett. B* **1998**, *428*, 105–114. [CrossRef]
2. Witten, E. Anti De Sitter Space and Holography. *Adv. Theor. Math. Phys.* **1998**, *2*, 253–291. [CrossRef]
3. Maldacena, J.M. The Large N limit of superconformal field theories and supergravity. *Adv. Theor. Math. Phys.* **1998**, *2*, 231–252. [CrossRef]
4. 't Hooft, G. A Planar Diagram Theory for Strong Interactions. *Nucl. Phys. B* **1974**, *72*, 461. [CrossRef]
5. Polchinski, J. *String Theory. Vol. 2: Superstring Theory and Beyond*; Cambridge Monographs on Mathematical Physics; Cambridge University Press: Cambridge, UK, 2007. [CrossRef]
6. Klebanov, I.R.; Strassler, M.J. Supergravity and a confining gauge theory: Duality cascades and chi SB resolution of naked singularities. *JHEP* **2000**, *08*, 052. [CrossRef]
7. Maldacena, J.M.; Nunez, C. Towards the large N limit of pure N = 1 superYang-Mills. *Phys. Rev. Lett.* **2001**, *86*, 588–591. [CrossRef] [PubMed]
8. Rey, S.J.; Yee, J.T. Macroscopic strings as heavy quarks in large N gauge theory and anti-de Sitter supergravity. *Eur. Phys. J. C* **2001**, *22*, 379–394. [CrossRef]
9. Maldacena, J.M. Wilson loops in large N field theories. *Phys. Rev. Lett.* **1998**, *80*, 4859–4862. [CrossRef]
10. Witten, E. Anti-de Sitter space, thermal phase transition, and confinement in gauge theories. *Adv. Theor. Math. Phys.* **1998**, *2*, 505–532. [CrossRef]
11. Hawking, S.W.; Page, D.N. Thermodynamics of Black Holes in anti-De Sitter Space. *Commun. Math. Phys.* **1983**, *87*, 577. [CrossRef]
12. Bernardini, A.E.; da Rocha, R. Entropic information of dynamical AdS/QCD holographic models. *Phys. Lett. B* **2016**, *762*, 107–115. [CrossRef]
13. Bernardini, A.E.; Braga, N.R.F.; da Rocha, R. Configurational entropy of glueball states. *Phys. Lett. B* **2017**, *765*, 81–85. [CrossRef]
14. Gleiser, M.; Stamatopoulos, N. Entropic Measure for Localized Energy Configurations: Kinks, Bounces, and Bubbles. *Phys. Lett. B* **2012**, *713*, 304–307. [CrossRef]
15. Gleiser, M.; Stamatopoulos, N. Information Content of Spontaneous Symmetry Breaking. *Phys. Rev. D* **2012**, *86*, 045004. [CrossRef]
16. Ferreira, L.F.; Da Rocha, R. Pion family in AdS/QCD: The next generation from configurational entropy. *Phys. Rev. D* **2019**, *99*, 086001. [CrossRef]
17. Karapetyan, G. Hadron multiplicity calculation: A configurational entropy approach to the saturation scale in QCD. *EPL* **2020**, *129*, 18002. [CrossRef]
18. D'Hoker, E.; Freedman, D.Z. Supersymmetric gauge theories and the AdS/CFT correspondence. In Proceedings of the Theoretical Advanced Study Institute in Elementary Particle Physics (TASI 2001): Strings, Branes and EXTRA Dimensions, Boulder, CO, USA, 3–29 June 2001; Volume 1, pp. 3–158.
19. Beisert, N.; Ahn, C.; Alday, L.F.; Bajnok, Z.; Drummond, J.M.; Freyhult, L.; Gromov, N.; Janik, R.A.; Kazakov, V.; Klose, T.; et al. Review of AdS/CFT Integrability: An Overview. *Lett. Math. Phys.* **2012**, *99*, 3–32. [CrossRef]
20. Ballon Bayona, C.A.; Boschi-Filho, H.; Braga, N.R.F.; Pando Zayas, L.A. On a Holographic Model for Confinement/Deconfinement. *Phys. Rev. D* **2008**, *77*, 046002. [CrossRef]
21. Susskind, L. The World as a hologram. *J. Math. Phys.* **1995**, *36*, 6377–6396. [CrossRef]
22. 't Hooft, G. Dimensional reduction in quantum gravity. *Conf. Proc. C* **1993**, *930308*, 284–296.
23. Brodsky, S.J.; de Teramond, G.F.; Dosch, H.G.; Erlich, J. Light-Front Holographic QCD and Emerging Confinement. *Phys. Rept.* **2015**, *584*, 1–105 . [CrossRef]

24. Brodsky, S.J.; de Teramond, G.F. Hadronic spectra and light-front wavefunctions in holographic QCD. *Phys. Rev. Lett.* **2006**, *96*, 201601. [CrossRef] [PubMed]
25. Polchinski, J.; Strassler, M.J. Hard scattering and gauge/string duality. *Phys. Rev. Lett.* **2002**, *88*, 031601. [CrossRef] [PubMed]
26. Polchinski, J.; Strassler, M.J. Deep inelastic scattering and gauge/string duality. *JHEP* **2003**, *05*, 012. [CrossRef]
27. Boschi-Filho, H.; Braga, N.R.F. Gauge/string duality and scalar glueball mass ratios. *JHEP* **2003**, *05*, 009. [CrossRef]
28. Boschi-Filho, H.; Braga, N.R.F. QCD/string holographic mapping and glueball mass spectrum. *Eur. Phys. J. C* **2004**, *32*, 529–533. [CrossRef]
29. Brodsky, S.J.; de Téramond, G.; Deur, A. AdS/QCD, Light-Front Holography, and the Nonperturbative Running Coupling. *Int. J. Mod. Phys. A* **2010**, *25*, 5009–5024. [CrossRef]
30. Brodsky, S.J.; de Téramond, G.F. Light-front hadron dynamics and AdS/CFT correspondence. *Phys. Lett. B* **2004**, *582*, 211–221. [CrossRef]
31. Issifu, A.; Brito, F.A. The (De)confinement Transition in Tachyonic Matter at Finite Temperature. *Adv. High Energy Phys.* **2019**, *2019*, 9450367. [CrossRef]
32. Issifu, A.; Brito, F.A. Confinement of fermions in tachyon matter. *Adv. High Energy Phys.* **2020**, *2020*, 1852841. [CrossRef]
33. Issifu, A.; Rocha, J.C.M.; Brito, F.A. Confinement of Fermions in Tachyon Matter at Finite Temperature. *Adv. High Energy Phys.* **2021**, *2021*, 6645678. [CrossRef]
34. Issifu, A.; Brito, F.A. An Effective Model for Glueballs and Dual Superconductivity at Finite Temperature. *Adv. High Energy Phys.* **2021**, *2021*, 5658568. [CrossRef]
35. Sen, A. Dirac-Born-Infeld action on the tachyon kink and vortex. *Phys. Rev. D* **2003**, *68*, 066008. [CrossRef]
36. Adolph, C.; Aghasyan, M.; Akhunzyanov, R.; Alexeev, M.G.; Alexeev, G.D.; Amoroso, A.; Andrieux, V.; Anfimov, N.V.; Anosov, V.; Augsten, K.; et al. Final COMPASS results on the deuteron spin-dependent structure function g_1^{d} and the Bjorken sum rule. *Phys. Lett. B* **2017**, *769*, 34–41. [CrossRef]
37. Deur, A.; Chen, J.P.; Kuhn, S.E.; Peng, C.; Ripani, M.; Sulkosky, V.; Adhikari, K.; Battaglieri, M.; Burkert, V.D.; Cates, G.D.; et al. Experimental study of the behavior of the Bjorken sum at very low Q2. *Phys. Lett. B* **2022**, *825*, 136878. [CrossRef]
38. Bjorken, J.D. Applications of the Chiral $U(6) \otimes U(6)$ Algebra of Current Densities. *Phys. Rev.* **1966**, *148*, 1467–1478. [CrossRef]
39. Bjorken, J.D. Inelastic Scattering of Polarized Leptons from Polarized Nucleons. *Phys. Rev. D* **1970**, *1*, 1376–1379. [CrossRef]
40. Deur, A.; Bosted, P.; Burkert, V.; Cates, G.; Chen, J.-P.; Choi, S.; Crabb, D.; de Jager, C.W.; De Vita, R.; Dodge, G.E.; et al. Experimental determination of the evolution of the Bjorken integral at low Q^2. *Phys. Rev. Lett.* **2004**, *93*, 212001. [CrossRef]
41. Deur, A.; Prok, Y.; Burkert, V.; Crabb, D.; Girod, F.X.; Griffioen, K.A.; Guler, N.; Kuhn, S.E.; Kvaltine, N. High precision determination of the Q^2 evolution of the Bjorken Sum. *Phys. Rev. D* **2014**, *90*, 012009. [CrossRef]
42. Abe, K.; Akagi, T.; Anthony, P.L.; Antonov, R.; Arnold, R.G.; Averett, T.; Band, H.R.; Bauer, J.M.; Borel, H.; Bosted, P.E.; et al. Measurements of the proton and deuteron spin structure functions g(1) and g(2). *Phys. Rev. D* **1998**, *58*, 112003. [CrossRef]
43. Ackerstaff, K.; Airapetian, A.; Akushevich, I.; Akopov, N.; Amarian, M.; Aschenauer, E.C.; Avakian, R.; Avakian, H.; Avetissian, A.; Bains, B.; et al. Measurement of the neutron spin structure function g1(n) with a polarized He-3 internal target. *Phys. Lett. B* **1997**, *404*, 383–389. [CrossRef]
44. Airapetian, A.; Akopov, N.; Akushevich, I.; Amarian, M.; Aschenauer, E.C.; Avakian, H.; Avakian, R.; Avetissian, A.; Bains, B.; Baumgarten, C.; et al. Measurement of the proton spin structure function g1(p) with a pure hydrogen target. *Phys. Lett. B* **1998**, *442*, 484–492. [CrossRef]
45. Airapetian, A.; Akopov, N.; Akopov, Z.; Andrus, A.; Aschenauer, E.C.; Augustyniak, W.; Avakian, R.; Avetissian, A.; Avetissian, E.; Belostotski, S.; et al. Precise determination of the spin structure function g(1) of the proton, deuteron and neutron. *Phys. Rev. D* **2007**, *75*, 012007. [CrossRef]
46. Anthony, P.L.; Arnold, R.G.; Averett, T.; Band, H.R.; Berisso, M.C.; Borel, H.; Bosted, P.E.; Bültmann, S.L.; Buenerd, M.; Chupp, T.; et al. Measurements of the Q^2 dependence of the proton and neutron spin structure functions $g(1)^p$ and $g(1)^n$. *Phys. Lett. B* **2000**, *493*, 19–28. [CrossRef]
47. Anthony, P.L.; Arnold, R.G.; Averett, T.; Band, H.R.; Berisso, M.C.; Borel, H.; Bosted, P.E.; Bültmann, S.L.; Buenerd, M.; Chupp, T.; et al. Measurement of the deuteron spin structure function $g1(d)(x)$ for $1 - (\mathrm{GeV/c})^2 < Q^2 < 40 - (\mathrm{GeV/c})^2$. *Phys. Lett. B* **1999**, *463*, 339–345. [CrossRef]
48. Anthony, P.L.; Arnold, R.G.; Band, H.R.; Borel, H.; Bosted, P.E.; Breton, V.; Button-Shafer, J.; Chen, J.P.; Chupp, T.E.; Clendenin, J.; et al. Deep inelastic scattering of polarized electrons by polarized He-3 and the study of the neutron spin structure. *Phys. Rev. D* **1996**, *54*, 6620–6650. [CrossRef]
49. Abe, K.; Akagi, T.; Anderson, B.D.; Anthony, P.L.; Arnold, R.G.; Averett, T.; Band, H.R.; Berisso, C.M.; Bogorad, P.; Borel, H.; et al. Precision determination of the neutron spin structure function g1(n). *Phys. Rev. Lett.* **1997**, *79*, 26–30. [CrossRef]
50. Deur, A.; Brodsky, S.J.; de Teramond, G.F. The QCD Running Coupling. *Nucl. Phys.* **2016**, *90*, 1. [CrossRef]
51. Olive, K.A.; Agashe, K.; Amsler, C.; Antonelli, M.; Arguin, J.-F.; Asner, D.M.; Baer, H.; Band, H.R.; Barnett, R.M.; Basaglia, T.; et al. Review of Particle Physics. *Chin. Phys. C* **2014**, *38*, 090001. [CrossRef]

52. Prosperi, G.M.; Raciti, M.; Simolo, C. On the running coupling constant in QCD. *Prog. Part. Nucl. Phys.* **2007**, *58*, 387–438. [CrossRef]
53. Altarelli, G. The QCD Running Coupling and its Measurement. *PoS* **2013**, *Corfu2012*, 002. [CrossRef]
54. Brodsky, S.J.; Pauli, H.C.; Pinsky, S.S. Quantum chromodynamics and other field theories on the light cone. *Phys. Rept.* **1998**, *301*, 299–486. [CrossRef]
55. Brodsky, S.J.; Deur, A.; Roberts, C.D. Artificial dynamical effects in quantum field theory. *Nat. Rev. Phys.* **2022**, *4*, 489–495. [CrossRef]
56. Dirac, P.A.M. Forms of Relativistic Dynamics. *Rev. Mod. Phys.* **1949**, *21*, 392–399. [CrossRef]
57. de Teramond, G.F.; Brodsky, S.J. Light-Front Holography and Gauge/Gravity Duality: The Light Meson and Baryon Spectra. *Nucl. Phys. B Proc. Suppl.* **2010**, *199*, 89–96. [CrossRef]
58. Brodsky, S.J.; de Teramond, G.F. Light-Front Dynamics and AdS/QCD Correspondence: The Pion Form Factor in the Space- and Time-Like Regions. *Phys. Rev. D* **2008**, *77*, 056007. [CrossRef]
59. Brodsky, S.J.; de Teramond, G.F. Light-Front Dynamics and AdS/QCD Correspondence: Gravitational Form Factors of Composite Hadrons. *Phys. Rev. D* **2008**, *78*, 025032. [CrossRef]
60. de Teramond, G.F.; Brodsky, S.J. Light-Front Holography: A First Approximation to QCD. *Phys. Rev. Lett.* **2009**, *102*, 081601. [CrossRef]
61. Abidin, Z.; Carlson, C.E. Gravitational form factors of vector mesons in an AdS/QCD model. *Phys. Rev. D* **2008**, *77*, 095007. [CrossRef]
62. Brodsky, S.J.; de Teramond, G.F.; Deur, A. Nonperturbative QCD Coupling and its β-function from Light-Front Holography. *Phys. Rev. D* **2010**, *81*, 096010. [CrossRef]
63. Karch, A.; Katz, E.; Son, D.T.; Stephanov, M.A. Linear confinement and AdS/QCD. *Phys. Rev. D* **2006**, *74*, 015005. [CrossRef]
64. Brodsky, S.J.; de Teramond, G.F. Applications of AdS/QCD and Light-Front Holography to Baryon Physics. *AIP Conf. Proc.* **2011**, *1388*, 22–33. [CrossRef]
65. Andreev, O.; Zakharov, V.I. Heavy-quark potentials and AdS/QCD. *Phys. Rev. D* **2006**, *74*, 025023. [CrossRef]
66. Born, M.; Infeld, L. Foundations of the new field theory. *Proc. Roy. Soc. Lond. A* **1934**, *144*, 425–451. [CrossRef]
67. Gibbons, G.W. Born-Infeld particles and Dirichlet p-branes. *Nucl. Phys. B* **1998**, *514*, 603–639. [CrossRef]
68. Dirac, P.A.M. An Extensible model of the electron. *Proc. Roy. Soc. Lond. A* **1962**, *268*, 57–67. [CrossRef]
69. Polchinski, J.; Chaudhuri, S.; Johnson, C.V. Notes on D-branes. *arXiv* **1996**, arXiv:hep-th/9602052. [CrossRef]
70. Polchinski, J. Tasi lectures on D-branes. In Proceedings of the Theoretical Advanced Study Institute in Elementary Particle Physics (TASI 96): Fields, Strings, and Duality, Boulder, CO, USA, 2–28 June 1996; Volume 11, pp. 293–356.
71. Taylor, W. Lectures on D-branes, gauge theory and M(atrices). In Proceedings of the 2nd Trieste Conference on Duality in String Theory, Trieste, Italy, 16–20 June 1997; Volume 6, pp. 192–271.
72. Sen, A. Stable nonBPS bound states of BPS D-branes. *JHEP* **1998**, *08*, 010. [CrossRef]
73. Sen, A. BPS D-branes on nonsupersymmetric cycles. *JHEP* **1998**, *12*, 021. [CrossRef]
74. Sen, A. Type I D particle and its interactions. *JHEP* **1998**, *10*, 021. [CrossRef]
75. Sen, A. Tachyon condensation on the brane anti-brane system. *JHEP* **1998**, *08*, 012. [CrossRef]
76. Recknagel, A.; Schomerus, V. Boundary deformation theory and moduli spaces of D-branes. *Nucl. Phys. B* **1999**, *545*, 233–282. [CrossRef]
77. Polchinski, J.; Thorlacius, L. Free fermion representation of a boundary conformal field theory. *Phys. Rev. D* **1994**, *50*, R622–R626. [CrossRef]
78. Callan, C.G.; Klebanov, I.R.; Ludwig, A.W.W.; Maldacena, J.M. Exact solution of a boundary conformal field theory. *Nucl. Phys. B* **1994**, *422*, 417–448. [CrossRef]
79. Sen, A. SO(32) spinors of type I and other solitons on brane-anti-brane pair. *JHEP* **1998**, *09*, 023. [CrossRef]
80. Harvey, J.A.; Kutasov, D.; Martinec, E.J. On the relevance of tachyons. *arXiv* **2000**, arXiv:hep-th/0003101. [CrossRef]
81. Majumder, J.; Sen, A. Vortex pair creation on brane-anti-brane pair via marginal deformation. *JHEP* **2000**, *06*, 010. [CrossRef]
82. Fendley, P.; Saleur, H.; Warner, N.P. Exact solution of a massless scalar field with a relevant boundary interaction. *Nucl. Phys. B* **1994**, *430*, 577–596. [CrossRef]
83. Kostelecky, V.A.; Samuel, S. The Static Tachyon Potential in the Open Bosonic String Theory. *Phys. Lett. B* **1988**, *207*, 169–173. [CrossRef]
84. Sen, A. Universality of the tachyon potential. *JHEP* **1999**, *12*, 027. [CrossRef]
85. Sen, A.; Zwiebach, B. Tachyon condensation in string field theory. *JHEP* **2000**, *03*, 002. [CrossRef]
86. Kostelecky, V.A.; Potting, R. Expectation values, Lorentz invariance, and CPT in the open bosonic string. *Phys. Lett. B* **1996**, *381*, 89–96. [CrossRef]
87. Moeller, N.; Sen, A.; Zwiebach, B. D-branes as tachyon lumps in string field theory. *JHEP* **2000**, *08*, 039. [CrossRef]
88. Harvey, J.A.; Kraus, P. D-Branes as unstable lumps in bosonic open string field theory. *JHEP* **2000**, *04*, 012. [CrossRef]

89. Moeller, N.; Taylor, W. Level truncation and the tachyon in open bosonic string field theory. *Nucl. Phys. B* **2000**, *583*, 105–144. [CrossRef]
90. Taylor, W. D-brane effective field theory from string field theory. *Nucl. Phys. B* **2000**, *585*, 171–192. [CrossRef]
91. Berkovits, N. The Tachyon potential in open Neveu-Schwarz string field theory. *JHEP* **2000**, *04*, 022. [CrossRef]
92. Berkovits, N.; Sen, A.; Zwiebach, B. Tachyon condensation in superstring field theory. *Nucl. Phys. B* **2000**, *587*, 147–178. [CrossRef]
93. Harvey, J.A.; Kraus, P.; Larsen, F.; Martinec, E.J. D-branes and strings as noncommutative solitons. *JHEP* **2000**, *07*, 042. [CrossRef]
94. Gopakumar, R.; Minwalla, S.; Strominger, A. Noncommutative solitons. *JHEP* **2000**, *05*, 020. [CrossRef]
95. Minahan, J.A.; Zwiebach, B. Effective tachyon dynamics in superstring theory. *JHEP* **2001**, *03*, 038. [CrossRef]
96. Gerasimov, A.A.; Shatashvili, S.L. On exact tachyon potential in open string field theory. *JHEP* **2000**, *10*, 034. [CrossRef]
97. Harvey, J.A.; Kraus, P.; Larsen, F. Exact noncommutative solitons. *JHEP* **2000**, *12*, 024. [CrossRef]
98. Dasgupta, K.; Mukhi, S.; Rajesh, G. Noncommutative tachyons. *JHEP* **2000**, *06*, 022. [CrossRef]
99. Kutasov, D.; Marino, M.; Moore, G.W. Some exact results on tachyon condensation in string field theory. *JHEP* **2000**, *10*, 045. [CrossRef]
100. Ghoshal, D.; Sen, A. Normalization of the background independent open string field theory action. *JHEP* **2000**, *11*, 021. [CrossRef]
101. Witten, E. Noncommutative Geometry and String Field Theory. *Nucl. Phys. B* **1986**, *268*, 253–294. [CrossRef]
102. Seiberg, N.; Witten, E. String theory and noncommutative geometry. *JHEP* **1999**, *09*, 032. [CrossRef]
103. Sen, A. Descent relations among bosonic D-branes. *Int. J. Mod. Phys. A* **1999**, *14*, 4061–4078. [CrossRef]
104. Bigazzi, F.; Cotrone, A.L. String theory meets QCD. *Frascati Phys. Ser.* **2012**, *54*, 378–385.
105. Issifu, A.; Brito, F.A. Phenomenology of strong interactions: Towards an effective theory for low energy QCD. *Eur. Phys. J. C* **2023**, *83*, 98. [CrossRef]
106. Taylor, W. Lectures on D-branes, tachyon condensation, and string field theory. In Proceedings of the School on Quantum Gravity, Valdivia, Chile, 4–14 January 2002; Volume 11, pp. 151–206. [CrossRef]
107. Banks, T.; Fischler, W.; Shenker, S.H.; Susskind, L. M theory as a matrix model: A Conjecture. *Phys. Rev. D* **1997**, *55*, 5112–5128. [CrossRef]
108. Witten, E. Bound states of strings and p-branes. *Nucl. Phys. B* **1996**, *460*, 335–350. [CrossRef]
109. Lust, D. Intersecting brane worlds: A Path to the standard model? *Class. Quant. Grav.* **2004**, *21*, S1399–S1424. [CrossRef]
110. Chatzistavrakidis, A.; Steinacker, H.; Zoupanos, G. Intersecting branes and a standard model realization in matrix models. *JHEP* **2011**, *09*, 115. [CrossRef]
111. Ibanez, L.E.; Marchesano, F.; Rabadan, R. Getting just the standard model at intersecting branes. *JHEP* **2001**, *11*, 002. [CrossRef]
112. Antoniadis, I.; Kiritsis, E.; Rizos, J.; Tomaras, T.N. D-branes and the standard model. *Nucl. Phys. B* **2003**, *660*, 81–115. [CrossRef]
113. Garousi, M.R. Tachyon couplings on nonBPS D-branes and Dirac-Born-Infeld action. *Nucl. Phys. B* **2000**, *584*, 284–299. [CrossRef]
114. Dymarsky, A.; Klebanov, I.R.; Roiban, R. Perturbative search for fixed lines in large N gauge theories. *JHEP* **2005**, *08*, 011. [CrossRef]
115. Gursoy, U.; Kiritsis, E. Exploring improved holographic theories for QCD: Part I. *JHEP* **2008**, *02*, 032. [CrossRef]
116. Gursoy, U.; Kiritsis, E.; Nitti, F. Exploring improved holographic theories for QCD: Part II. *JHEP* **2008**, *02*, 019. [CrossRef]
117. Grigoryan, H.R.; Radyushkin, A.V. Form Factors and Wave Functions of Vector Mesons in Holographic QCD. *Phys. Lett. B* **2007**, *650*, 421–427. [CrossRef]
118. Bigazzi, F.; Casero, R.; Cotrone, A.L.; Kiritsis, E.; Paredes, A. Non-critical holography and four-dimensional CFT's with fundamentals. *JHEP* **2005**, *10*, 012. [CrossRef]
119. Gursoy, U.; Kiritsis, E.; Mazzanti, L.; Nitti, F. Holography and Thermodynamics of 5D Dilaton-gravity. *JHEP* **2009**, *05*, 033. [CrossRef]
120. Iatrakis, I.; Kiritsis, E.; Paredes, A. An AdS/QCD model from Sen's tachyon action. *Phys. Rev. D* **2010**, *81*, 115004. [CrossRef]
121. Barbosa-Cendejas, N.; Cartas-Fuentevilla, R.; Herrera-Aguilar, A.; Mora-Luna, R.R.; da Rocha, R. Dynamical tachyonic AdS/QCD and information entropy. *Phys. Lett. B* **2018**, *782*, 607–612. [CrossRef]
122. Bajnok, Z.; Drukker, N.; Hegedüs, A.; Nepomechie, R.I.; Palla, L.; Sieg, C.; Suzuki, R. The spectrum of tachyons in AdS/CFT. *JHEP* **2014**, *03*, 055. [CrossRef]
123. Nayak, G.C. Renormalization Group Equation and QCD Coupling Constant in the Presence of SU(3) Chromo-Electric Field. *Eur. Phys. J. C* **2009**, *64*, 73–79. [CrossRef]
124. Tong, D. String Theory. *arXiv* **2009**, arXiv:0908.0333.
125. Schechter, J. Effective Lagrangian with two color-singlet gluon fields. *Phys. Rev. D* **1980**, *21*, 3393–3400. [CrossRef]
126. Carter, G.W.; Scavenius, O.; Mishustin, I.N.; Ellis, P.J. An Effective model for hot gluodynamics. *Phys. Rev. C* **2000**, *61*, 045206. [CrossRef]
127. Campbell, B.A.; Ellis, J.R.; Olive, K.A. QCD Phase Transitions in an Effective Field Theory. *Nucl. Phys. B* **1990**, *345*, 57–78. [CrossRef]
128. Kochelev, N. Ultralight glueballs in Quark-Gluon Plasma. *Phys. Part. Nucl. Lett.* **2016**, *13*, 149–156. [CrossRef]

129. Kharzeev, D.; Levin, E.; Tuchin, K. Classical gluodynamics in curved space-time and the soft pomeron. *Phys. Lett. B* **2002**, *547*, 21–30. [CrossRef]
130. Mack, G. D-independent representation of Conformal Field Theories in D dimensions via transformation to auxiliary Dual Resonance Models. Scalar amplitudes. *arXiv* **2009**, arXiv:0907.2407. [CrossRef]
131. Cornwall, J.M. Dynamical Mass Generation in Continuum QCD. *Phys. Rev. D* **1982**, *26*, 1453. [CrossRef]
132. Amoretti, A.; Magnoli, N. Conformal perturbation theory. *Phys. Rev. D* **2017**, *96*, 045016. [CrossRef]
133. Deur, A.; Burkert, V.; Chen, J.P.; Korsch, W. Experimental determination of the effective strong coupling constant. *Phys. Lett. B* **2007**, *650*, 244–248. [CrossRef]
134. Megias, E.; Pirner, H.J.; Veschgini, K. QCD thermodynamics using five-dimensional gravity. *Phys. Rev. D* **2011**, *83*, 056003. [CrossRef]
135. de Paula, W.; Frederico, T.; Forkel, H.; Beyer, M. Dynamical AdS/QCD with area-law confinement and linear Regge trajectories. *Phys. Rev. D* **2009**, *79*, 075019. [CrossRef]
136. Afonin, S.S. Holographic like models as a five-dimensional rewriting of large-Nc QCD. *Int. J. Mod. Phys. A* **2010**, *25*, 5683–5710. [CrossRef]
137. Ochs, W. The Status of Glueballs. *J. Phys. G* **2013**, *40*, 043001. [CrossRef]
138. Crede, V.; Meyer, C.A. The Experimental Status of Glueballs. *Prog. Part. Nucl. Phys.* **2009**, *63*, 74–116. [CrossRef]
139. Cornwall, J.M.; Soni, A. Glueballs as Bound States of Massive Gluons. *Phys. Lett. B* **1983**, *120*, 431. [CrossRef]
140. Shirkov, D.V. On the QCD coupling behavior in the infrared region. *Theor. Math. Phys.* **2002**, *132*, 1309–1319. [CrossRef]
141. Nakamura, K.; Hagiwara, K.; Hikasa, K.; Murayama, H.; Tanabashi, M.; Watari, T.; Amsler, C.; Antonelli, M.; Asner, D.M.; Baer, H.; et al. Review of particle physics. *J. Phys. G* **2010**, *37*, 075021. [CrossRef]
142. Lucini, B.; Moraitis, G. The Running of the coupling in SU(N) pure gauge theories. *Phys. Lett. B* **2008**, *668*, 226–232. [CrossRef]
143. Simonov, Y.A. Perturbative theory in the nonperturbative QCD vacuum. *Phys. Atom. Nucl.* **1995**, *58*, 107–123.
144. Badalian, A.M.; Veselov, A.I.; Bakker, B.L.G. Restriction on the strong coupling constant in the IR region from the 1D-1P splitting in bottomonium. *Phys. Rev. D* **2004**, *70*, 016007. [CrossRef]
145. Badalian, A.M.; Kuzmenko, D.S. A Short distance quark - anti-quark potential. *Phys. Atom. Nucl.* **2004**, *67*, 561–563. [CrossRef]
146. Badalian, A.M.; Morgunov, V.L. Determination of alpha(s)(1-GeV) from the charmonium fine structure. *Phys. Rev. D* **1999**, *60*, 116008. [CrossRef]
147. Simonov, Y.A. Asymptotic freedom and IR freezing in QCD: The role of gluon paramagnetism. *Phys. Atom. Nucl.* **2011**, *74*, 1223. [CrossRef]
148. Badalian, A.M.; Veselov, A.I.; Bakker, B.L.G. The Pole and heavy quark masses in the Hamiltonian approach. *Phys. Atom. Nucl.* **2004**, *67*, 1367–1377. [CrossRef]
149. Badalian, A.M.; Veselov, A.I. The Static force in background perturbation theory. *Phys. Atom. Nucl.* **2005**, *68*, 582–590. [CrossRef]
150. Badalian, A.M.; Kuzmenko, D.S. Freezing of QCD coupling alpha(s) affects the short distance static potential. *Phys. Rev. D* **2001**, *65*, 016004. [CrossRef]
151. Badalian, A.M. Strong coupling constant in coordinate space. *Phys. Atom. Nucl.* **2000**, *63*, 2173–2183. [CrossRef]
152. Kondo, K.I. Vacuum condensates, effective gluon mass and color confinement in the large N(c) expansion. *arXiv* **2003**, arXiv:hep-th/0307270.